Research Square

Preprints are preliminary reports that have not undergone peer review.
They should not be considered conclusive, used to inform clinical practice,
or referenced by the media as validated information.

# Divergent Drought Propagation Pathways in Adjacent Mediterranean Lakes Under Identical Climatic Forcing: Satellite-Based Attribution of Land Cover–Hydrology Interactions

**Ali Muslim AMIRI**
Bursa Uludağ Üniversitesi
**Feza ÖRÜÇ**
karaer@uludag.edu.tr

Bursa Uludağ Üniversitesi

**Research Article**

**Keywords:** Drought propagation, Hydrological drought attribution, Standardized Lake Level Index, Evaporative demand, Satellite altimetry, Mediterranean lakes

**Posted Date:** August 7th, 2026

**DOI:** https://doi.org/10.21203/rs.3.rs-10457346/v1

**License:** This work is licensed under a Creative Commons Attribution 4.0 International License.
Read Full License

**Additional Declarations:** No competing interests reported.

**Version of Record:** A version of this preprint was published at Sustainable Water Resources Management on October 23rd, 2026. See the published version at https://doi.org/10.1007/s40899-026-01413-w.

# Divergent Drought Propagation Pathways in Adjacent Mediterranean Lakes Under Identical Climatic Forcing: Satellite-Based Attribution of Land Cover–Hydrology Interactions

Ali Muslim AMIRI[1,2*], Feza ÖRÜÇ[1*]

[1] Environmental Engineering Department, Engineering Faculty, Bursa Uludag University, 16059 Nilufer/Bursa, Türkiye

[2] Water and Environmental Engineering Department, Mining and Environment Faculty, Balkh University, 1701 Mazar-i-Sharif/Balkh, Afghanistan

* Corresponding author: karaer@uludag.edu.tr [0000-0002-2986-0114]

* Corresponding author: alimuslimamiri@yahoo.com [0009-0007-6280-8899]

**Abstract**

Lakes İznik and Uluabat, ~50 km apart in northwestern Turkey, share the same regional precipitation regime and evaporative demand, yet followed markedly different hydrological drought trajectories between 1993 and 2024. Using this natural experiment, we present a transferable, satellite-only attribution framework for separating climatic from anthropogenic drivers of lake-level drought, requiring no in-situ discharge data. Meteorological drought was quantified using the Standardized Precipitation Index (SPI) and Standardized Precipitation-Evapotranspiration Index (SPEI), computed from satellite precipitation and potential evapotranspiration products; hydrological drought was tracked via a Standardized Lake Level Index (SLLI) built from bias-corrected altimetric and gauge records. Propagation from meteorological to hydrological drought was assessed through lagged correlation, event matching, regression-based attribution, and Granger causality, while land-cover change was mapped using a 30-m global dataset (1985–2022).

Precipitation showed no significant trend at either lake, whereas potential evapotranspiration rose significantly at both sites, widening the climatic water deficit and roughly doubling SPEI-based drought frequency after 2000, identifying evaporative demand rather than rainfall decline as the primary post-2000 driver. Basin morphology governed propagation timescale: the shallow, flow-through Uluabat responded within ~2 months of meteorological forcing, while the deep, closed-basin İznik integrated forcing over 9–10 months, with causality confirmed only at longer lags. Despite opposing land-cover trajectories, agricultural contraction and afforestation at İznik versus stable cropland and river abstraction at Uluabat, both lakes showed statistically comparable rates of non-climatic hydrological decline. These findings offer a scalable diagnostic tool for water managers in data-scarce lake basins across Central Asia, East Africa, and the Tibetan Plateau.

**Keywords**: Drought propagation, Hydrological drought attribution, Standardized Lake Level Index, Evaporative demand, Satellite altimetry, Standardized drought indices, Mediterranean lakes

## 1. Introduction

Lakes are among the most visible recorders of planetary water stress. In the most comprehensive satellite-based inventory to date, covering more than 1,900 large lakes between 1992 and 2020, Yao et al. (2023) demonstrated that nearly two-thirds of Earth's large water bodies have lost storage volume, with the livelihoods and water security of approximately two billion people already affected. Yet global loss statistics, striking as they are, obscure a deeper and more practically urgent question: why do specific lakes decline? Precipitation (PCP) deficits, intensifying evaporative demand, and anthropogenic water withdrawal rarely act in isolation. They interact, compound, and in some systems, cancel each other out. Partitioning these contributions, conducting rigorous attribution at the individual lake scale, is not merely a scientific exercise. It is a prerequisite for adaptive water management, particularly in semi-arid Mediterranean regions where anthropogenic and climatic pressures co-evolve and where both are projected to intensify over the coming decades (IPCC, 2021; Soydan, 2026; Zhao et al., 2025).

The conceptual backbone of any lake-scale attribution effort is drought propagation: the process by which an atmospheric moisture deficit, whether expressed as reduced precipitation, enhanced evaporative demand, or both, is transmitted through the terrestrial water cycle and eventually manifests as a deficit in soil moisture, streamflow, groundwater, or lake level (Dai et al., 2025; Xiong et al., 2025; Zhou et al., 2024). This propagation is neither instantaneous nor linear. Van Loon et al. (2024), in a comprehensive interdisciplinary review, reframed drought not as a discrete event but as a hydrological-ecological-social continuum, in which memory effects at multiple timescales mediate the cascading transfer of impacts across interconnected systems. The practical consequence for attribution is significant: in basins with substantial hydrological memory, the coupling between contemporaneous climatic forcing and observed lake-level anomalies may be temporally diffuse or spatially attenuated, potentially obscuring the actual drivers of decline. Recent empirical analyses confirm that catchment baseflow index, vegetation coverage, soil water-holding capacity, and topographic slope collectively modulate how efficiently a meteorological deficit translates into a hydrological one (Xiong et al., 2025; Zhou et al., 2024).

Among these modulators, land use and land cover change has received comparatively little systematic attention at the lake scale, despite growing mechanistic evidence that afforestation, agricultural contraction, and urban expansion fundamentally restructure basin-scale runoff generation, groundwater recharge rates, and the seasonal partitioning of evapotranspiration (Dai et al., 2025; Li et al., 2024; Shadmehri Toosi et al., 2025). This is a consequential gap. Two lakes sharing identical climatic forcing may experience entirely different hydrological drought trajectories if their catchments have followed divergent land cover pathways, not because climate matters less, but because the basin-scale filters that determine how climate signals are transmitted to lake levels differ. Exploiting this logic as a formal attribution framework, using geographically adjacent lakes as natural analogues of a controlled experiment, is a methodological opportunity that remains largely underused in the limnological and applied hydrology literature (Li et al., 2024; Luo et al., 2024).

A parallel shortcoming limits the reliability of drought characterisation itself. The Standardized Precipitation Evapotranspiration Index (SPEI; Vicente-Serrano et al., 2010) is theoretically superior to the precipitation-only Standardized Precipitation Index (SPI; WMO, 2012) in environments where evaporative demand strongly modulates drought dynamics (Abu Arra & Şişman, 2024), yet it is almost universally computed using potential evapotranspiration (PET) derived from the Thornthwaite method, a formulation that relies solely on air temperature and systematically underestimates demand under the high

vapour pressure deficits, strong radiation loading, and significant wind forcing characteristic of Mediterranean summers (Gumus & Seker, 2024; Lee et al., 2024; Nwayor & Robeson, 2024). The recently published GLEAM4 dataset (Miralles et al., 2025) addresses this limitation through a Penman-based PET formulation calibrated against global eddy-covariance and sap-flow observations, delivering daily estimates at 0.1° spatial resolution from 1980 to the present with substantially improved representation of canopy interception, vapour pressure-driven demand, and plant access to groundwater. Critically, in a companion runoff calibration study for the İznik Lake Basin using gradient boosting decision trees, Amiri & Örüç (2026) demonstrated quantitatively that GLEAM4-derived PET outperforms ERA5-Land PET in reproducing observed catchment hydrology in this specific study region, providing direct, site-validated empirical support for its adoption here. To our knowledge, however, GLEAM4 has not previously been applied in the context of Mediterranean lake drought attribution, making this its first deployment for that purpose.

The Mediterranean basin is consistently identified as one of the world's most climatically vulnerable regions, where hydrological consequences of anthropogenic warming are already measurable and are projected to accelerate (Eekhout et al., 2025; Rezaei et al., 2024; Seager et al., 2024). The record-breaking 2022 European drought, for instance, was shown to have had more than 30% of its intensity and spatial extent attributable to human-induced warming operating through enhanced evapotranspiration, with antecedent soil drying accounting for a further 14–41% of the climate change contribution (Bevacqua et al., 2024). More broadly, rising temperatures are now the primary accelerant of drought severity globally, shifting drought dynamics towards evaporative-demand dominance even in regions where PCP has not declined significantly (Gebrechorkos et al., 2025). Situated at the north-eastern edge of this climatically stressed region, north-western Turkey hosts lake systems facing compounding pressures from rising evaporative demand, variable precipitation, and structural land-use change. While prior studies have documented significant water-level declines in Lakes İznik and Uluabat (Erkoç et al., 2024; Tagil, 2007), neither the mechanistic drivers of these trajectories nor the degree to which divergent land cover change, rather than shared climate variability, explains their differences, has been quantitatively established.

This gap is particularly striking given the analytical opportunity the two lakes offer. Lakes İznik and Uluabat are located in the Marmara region of north-western Turkey, separated by approximately 50 km, and share the same regional PCP regime and atmospheric evaporative demand. Yet over the period 1993–2024 they have followed fundamentally different hydrological drought trajectories. Lake İznik is a deep, closed-basin tectonic lake (maximum depth ~80 m; catchment-to-lake area ratio ~5.7) subject to regulated abstraction for drinking water supply. Lake Uluabat, a Ramsar-designated wetland, is an extremely shallow, flow-through system (mean depth ~2 m; catchment-to-lake area ratio ~40) whose hydrology is closely coupled to agricultural drainage from a large watershed. Their contrasting morphologies, hydrological connectivities, and land-cover trajectories, the İznik basin underwent a 13.3% agricultural expansion alongside a net decline in tree/forest cover of 36.9 km² over 2000–2022, while Uluabat's cropland remained the overwhelmingly dominant class with only marginal change (+1.7%), and its forest cover declined more sharply in relative terms (−7.0%), constitute a natural experiment of considerable analytical value. Although both basins exhibit directionally similar land-cover shifts, the substantially greater magnitude of agricultural expansion at İznik and the contrasting dominance of direct river abstraction at Uluabat generate mechanistically distinct anthropogenic pressures on the lake water balance. When two lakes under equivalent climatic forcing diverge in their drought responses, the divergence is attributable to basin structure, land-cover intensity, and abstraction regime rather than to

differential climate, providing a tractable basis for attribution without requiring counterfactual model simulations.

This study exploits this natural experiment through three original contributions. First, it provides the initial application of GLEAM4 satellite-derived PET in Mediterranean lake drought attribution, enabling physically consistent SPEI calculations that overcome the systematic biases inherent in temperature-only PET formulations and revealing, for the first time in this regional context, that rising evaporative demand rather than declining PCP is the primary driver of post-2000 drought intensification at both lakes. Second, it develops and demonstrates a dual-lake natural experiment framework, with Lakes İznik and Uluabat serving as hydraulically independent, climatologically equivalent systems with markedly divergent land cover and morphological histories, as a transferable attribution approach for disentangling climatic from anthropogenic drivers of hydrological drought. Propagation is quantified through a multi-method framework combining lagged cross-correlation, event-based matching, ordinary least squares (OLS) attribution with Newey–West HAC inference, and Granger causality analysis, applied to a 384-month composite lake level record assembled from bias-corrected satellite altimetry and in-situ gauge data. Third, the study introduces a new operationalization of propagation efficiency index (PEI), which quantifies the fraction of meteorological drought events that propagate to the hydrological domain. As a dimensionless and normalized measure, PEI is suitable for cross-system comparison of drought propagation fidelity across lakes and basins. The all-satellite framework, drawing on CHIRPS v3, GLEAM4, HydroWeb/Sentinel-3, Landsat, and GLC_FCS30D, requires no in-situ discharge records and is directly transferable to lake pairs in Central Asia, East Africa, and the Tibetan Plateau, where attribution challenges of comparable complexity exist alongside sparse ground-based monitoring infrastructure.

## 2. Data and methods

### 2.1. Study area

Lakes Iznik (40.43°N, 29.56°E) and Uluabat (40.17°N, 28.60°E) are located in the Marmara region of north-western Turkey, separated by approximately 50 km and lying within the same regional climate zone (Figure 1). Mean annual precipitation (PCP) across the region ranges from 650 to 700 mm, with characteristically dry summers and mild, rainy winters typical of a Mediterranean transitional climate. The close geographical proximity of the two lakes ensures that they receive effectively identical PCP inputs and experience the same regional temperature and evaporative demand regimes, a condition that constitutes the fundamental premise of the natural experiment design adopted in this study. When two lakes sharing the same climatic forcing display markedly different hydrological drought trajectories, the divergence cannot be attributed to differential climate and must instead reflect differences in basin morphology, land cover, or human water use.

The two lakes are morphologically and functionally contrasting in ways that are analytically consequential (Table 1). Lake Iznik is a deep tectonic lake (Gastineau et al., 2024) occupying a closed basin (maximum depth approximately 80 m; surface area approximately 298 km²) with a catchment of approximately 1,700 km² and a catchment-to-lake area ratio of approximately 5.7. It serves as a drinking water reserve and is subject to regulated water abstraction. Lake Uluabat (Apolyont), designated as a Ramsar Wetland in 1998 (Elmaci et al., 2008), is an extremely shallow lake (surface area approximately 135 km²; mean depth approximately 2 m) fed primarily by the Mustafakemalpaşa River from a substantially larger catchment of approximately 5,400 km² (ratio approximately 40). Its hydrological

connectivity is closely coupled to agricultural drainage across this expansive watershed. This structural contrast, deep buffering versus shallow exposure, modest versus expansive catchment, and abstraction-managed versus agriculturally dominated inflow, constitutes the scientific focal point of the study and is precisely what enables a dual-lake attribution framework to function as an analogue to a controlled experiment.

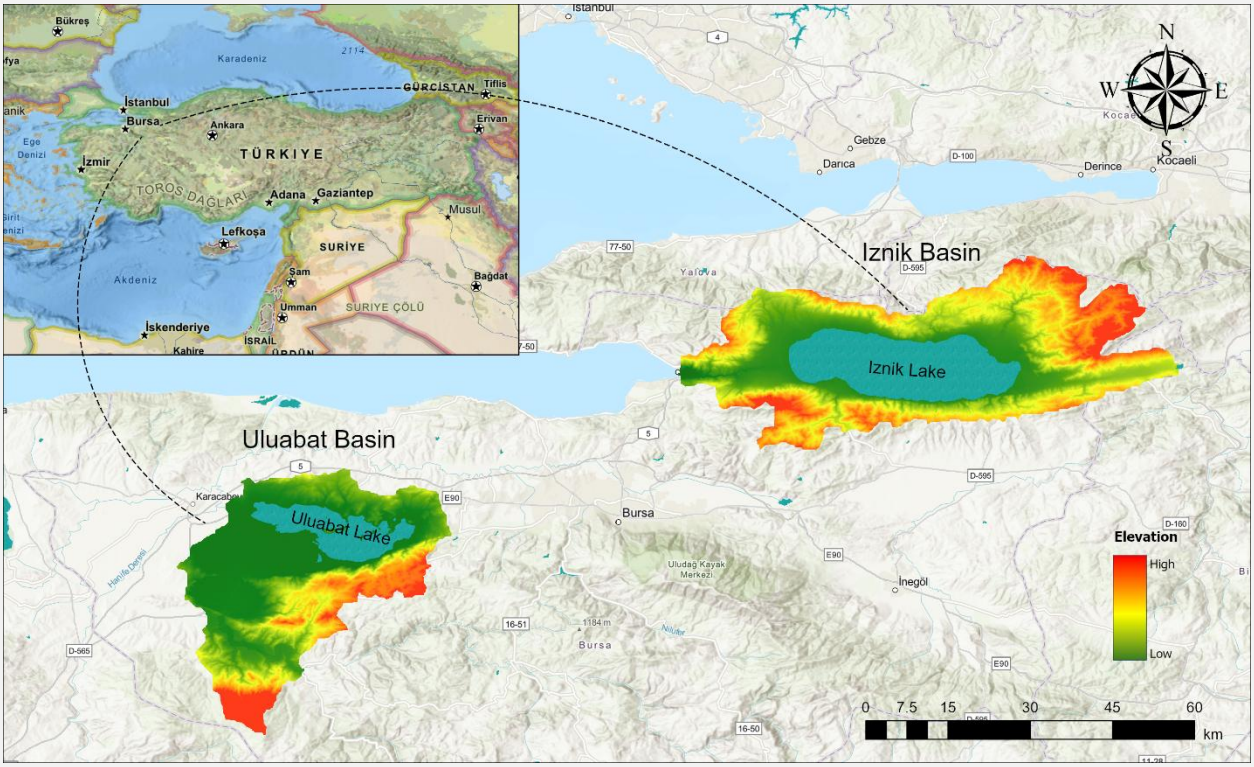


*Figure 1. Location of the study area in Turkey and the SRTM-derived Digital Elevation Model (DEM). The Iznik Basin (northeast) and Uluabat Basin (southwest) in the Marmara Region are outlined on the DEM. Elevation ranges from low (green) to high (red).*

*Table 1. Key morphological and catchment characteristics of Lakes Iznik and Uluabat.*

| **Parameter** | **Lake Iznik** | **Lake Uluabat** |
|---|---|---|
| Surface area (km²) | ~298 | ~135 |
| Maximum depth (m) | ~80 | ~2–3 |
| Basin type | Closed (Semi-closed) | Semi-closed/drainage-connected |
| Catchment area (km²) | ~1,700 | ~5,400 |
| Catchment:lake area ratio | ~5.7 | ~40 |
| Human abstraction | High (agriculture + industry) | Moderate (agricultural drainage) |
| Conservation status | Drinking water reserve | Ramsar Wetland (1998) |
| Dominant inflow type | Direct precipitation + surface runoff | River inflow (Mustafakemalpaşa R.) |

### 2.2. Data sources and preprocessing

All primary data used in this study are satellite-derived, a deliberate design choice that eliminates dependence on ground-based monitoring networks and ensures the framework's transferability to data-scarce regions globally. Table 2 summarises the complete data inventory.

For meteorological drought characterisation, monthly PCP was obtained from CHIRPS v3, 1981–present, land-only, high-resolution (0.05°) gridded PCP dataset released in early 2025 that incorporates multiple improvements over its predecessor (Funk et al., 2026), CHIRPS v2, including an expanded range of input data sources, improved PCP variance estimation, and an updated CHPclim2 climatology (Climate Hazards Center, 2025; doi:10.15780/G2JQ0P). Monthly PCP values were spatially averaged over each lake's delineated catchment polygon. Daily potential evapotranspiration (PET) was obtained from the GLEAM4 dataset (0.1° spatial resolution; 1980–present), which employs a Penman-based PET formulation and hybrid machine learning to represent evaporative stress, interception, and soil moisture constraints (Miralles et al., 2025). Daily GLEAM4 PET values were aggregated to monthly totals and spatially averaged over each catchment, providing the PET input for SPEI computation. The superiority of this approach over Thornthwaite temperature-only PET methods is well established in the literature (Amiri & Örüç, 2026; Bouabdelli et al., 2025; Vicente-Serrano et al., 2022).

*Table 2. Data sources and derived variables used in this study.*

| Variable | Dataset | Period | Resolution | Use in Study |
|---|---|---|---|---|
| Precipitation | CHIRPS v3 | 1981–present | 0.05°/monthly | SPI, SPEI input |
| PET / actual ET | GLEAM4 | 1980–present | 0.1°/daily | SPEI input (novel application) |
| Lake water level | HydroWeb + Sentinel-3 OLTC | 1993–present | Monthly | SLLI computation |
| Lake water level (validation) | DSİ in-situ gauges | 2004–2015 | Monthly | Bias correction/cross-validation |
| Lake surface area | Landsat 5/7/8/9 imagery | 1993–2024 | 30 m | SLLI physical validation |
| Land use/land cover | GLC_FCS30D | 2000–2022 | 30 m | Attribution analysis |

Lake water levels were assembled from three sources to produce a continuous monthly time series spanning 1993–2024: HydroWeb satellite altimetry (1993–2003), observations from the Turkish State Hydraulic Works (DSİ) in-situ gauge network (2004–2024), and Sentinel-3 Open Loop Tracking Command (OLTC) altimetry data (2016–2024). At each inter-source transition point, a linear regression error correction of the form was applied, and the corrected series were validated using Pearson's r, Root Mean Square Error (RMSE), and Nash–Sutcliffe Efficiency (NSE). Segment discontinuities exceeding the threshold were resolved through an additional cumulative offset correction. Land cover change was monitored using the GLC_FCS30D product at 30 m annual resolution (Zhang et al., 2024) for 2000–2022. The original GLC-FCS30D land-cover classes were harmonized into seven generalized categories (Water, Trees/Forest, Flooded Vegetation, Cropland, Built-up, Bare Ground, and Rangeland/Shrub/Grass) to facilitate long-term comparison and statistical analysis. Lake surface area dynamics were assessed

using Landsat (5/7/8/9)-derived Normalised Difference Water Index (NDWI) anomalies at 30 m spatial resolution for 1993–2024 as an independent physical validation layer.

## 2.3. Meteorological drought indices

### *2.3.1. Standardized precipitation index (SPI)*

The Standardized Precipitation Index (SPI; Mckee et al., 1993) was computed at 1-, 3-, 6-, 12-, and 24-month accumulation timescales in accordance with world meteorological organization guidelines (WMO, 2012). A two-parameter Gamma distribution was fitted to the rolling monthly PCP totals at each catchment-averaged grid cell. Because the Gamma distribution is undefined for zero-precipitation months, the empirical probability of zero precipitation ($q$) was incorporated through a mixed probability model, yielding a combined cumulative distribution function (CDF):

$$H(x) = q + (1-q) \cdot F_{\Gamma}(x) \qquad \textit{Equation 1}$$

where $F_{\Gamma}$ is the standard cumulative Gamma CDF. The resulting cumulative probabilities were transformed to the standard normal distribution via a probit transformation to obtain SPI values:

$$\mathrm{SPI} = \Phi^{-1}[H(x)] \qquad \textit{Equation 2}$$

Distributional goodness-of-fit was validated at each grid cell using the Kolmogorov–Smirnov (KS) test at a 5% significance level (Chandy et al., 2026; Massey, 1951).

### *2.3.2. Standardized precipitation evapotranspiration index (SPEI)*

The SPEI (Vicente-Serrano et al., 2010) was computed over the same five timescales using the monthly climatic water balance $D = P - \mathrm{PET}$, where $P$ is CHIRPS v3 PCP and $PET$ is GLEAM4-derived monthly potential evapotranspiration. Because the $D$ series takes negative values, a three-parameter log-logistic distribution was fitted to the shifted series (minimum shifted above $10^{-6}$ for each calendar month), following the approach of Stagge et al. (2015) with maximum likelihood estimation (MLE). The cumulative probabilities of this distribution were then transformed to the standard normal to yield SPEI values:

$$\mathrm{SPEI} = \Phi^{-1}[F_{\mathrm{LL}}(D)] \qquad \textit{Equation 3}$$

The integration of GLEAM4 represents a substantive methodological advance over prior drought studies in the region. GLEAM4 employs Penman's equation, incorporating surface net radiation, near-surface air temperature, wind speed, vapour pressure deficit, and leaf area index, to estimate PET, rather than the temperature-only Thornthwaite formulation that systematically underestimates PET in semi-arid environments (Ramachandran et al., 2026). GLEAM4 additionally incorporates hybrid machine learning to represent evaporative stress, canopy interception for both tall and short vegetation, and plant access to groundwater (Miralles et al., 2025), providing a substantially more process-consistent representation of atmospheric water demand in Mediterranean settings.

### *2.3.3. Distribution fitting and goodness-of-fit assessment*

Kolmogorov-Smirnov goodness-of-fit tests verified that the selected distributions, gamma for SPI and log-logistic for SPEI, adequately represent the climatic data across all timescales for both lakes, satisfying

WMO criteria. This validation provides a statistically robust foundation for the subsequent drought characterisation (detailed statistics are provided in Supplementary Section (S1.1) and Table S1).

## 2.4. Hydrological drought index: standardized lake level index (SLLI)

### *2.4.1. Composite lake level series construction*

Because in-situ gauge records contain temporal gaps, a composite best-available lake level series was constructed by integrating DSİ observations with bias-corrected satellite and DAHITI altimetric data. The bias-correction algorithm, data integration priority scheme, and source-weighting procedure are described in Supplementary Section S1.2-S1.4.

The Standardized Lake Level Index (SLLI) was derived from the composite monthly series using a calendar-month empirical standardization approach. For each of the twelve calendar months independently, lake level observations were ranked in ascending order and assigned non-exceedance probabilities via:

$$p_{i,j} = \frac{i + 0.5}{n_j + 1} \qquad \textit{Equation 4}$$

where $i$ is the ascending rank and $n$ is the non-missing sample size for that calendar month. Each probability was then transformed to a z-score through the inverse standard normal distribution (probit transform). This distribution-free approach avoids parametric assumptions that are frequently violated by lake level series subject to threshold hydraulic behavior or anthropogenic regulation. SLLI values of $\leq -1.0$, $\leq -1.5$, and $\leq -2.0$ denote moderate, severe, and extreme lake-level drought, respectively, consistent with the SPI/SPEI classification of Mckee et al. (1993). Composite-derived SLLI values were validated against gauge-only SLLI over their concurrent period using Pearson correlation.

## 2.5. Independent cross-validation: NDWI-based surface water index

Monthly median NDWI composites were standardized using the same calendar-month empirical procedure (Equation 4) to produce the Standardized NDWI Index (SNDWI). The SNDWI provides an independent, remotely sensed indicator of lake surface water anomaly against which SLLI was cross-validated. Agreement was assessed using (i) Pearson and Spearman correlation coefficients, (ii) lagged cross-correlation at offsets 0 – 12 months, and (iii) binary drought-period contingency statistics, precision, recall, and F1 score, computed at the shared drought threshold of $\leq -1.0$ for both indicators.

## 2.6. Drought propagation framework

Meteorological-to-hydrological drought propagation at each lake was quantified using a three-tier analytical framework applied to all SPI/SPEI timescale–SLLI pairs. Stationarity of all input series was first verified using augmented Dickey–Fuller (ADF) and KPSS tests.

### *2.6.1. Lagged cross-correlation*

Pearson correlation between each meteorological index and SLLI was computed at lags 0–24 months (index leading SLLI). Because temporal autocorrelation inflates nominal degrees of freedom, all p-values and confidence intervals (CI) were estimated using an effective sample size (ESS) correction (Bretherton et al., 1999). Significance was additionally evaluated against AR(1)-preserving Monte Carlo surrogates ($n$ = 499) to guard against spurious association arising from persistence structure alone. The Benjamini &

Hochberg (1995) false discovery rate (FDR) procedure was applied across the full lag spectrum. The dominant meteorological driver at each lake was identified as the SPI/SPEI timescale yielding the largest surrogate-significant FDR-corrected lagged correlation.

#### *2.6.2. Event-based propagation and propagation efficiency index (PEI)*

Following Mckee et al. (1993), drought onset events were defined by the index crossing below −0.84 (≈ 20th percentile), a threshold widely used to identify the initiation of below-normal conditions in propagation studies. This threshold is distinct from the −1.0 classification boundary and was selected specifically to maximise detection sensitivity for onset events. Onsets were identified as the first month in which the index fell below −0.84 after a period of non-drought conditions; the procedure was applied separately to the dominant meteorological index and to the SLLI.

To provide a dimensionless, basin-size-independent measure of signal transfer fidelity, we define the Propagation Efficiency Index (PEI):

$$PEI = n_{matched} / n_{met} \qquad \textit{Equation 5}$$

where $n_{met}$ is the total number of meteorological drought onset events and $n_{matched}$ is the count of those onsets for which at least one SLLI onset occurred within the forward window [$t_0$, $t_0$ + 24 months]. The 24-month horizon is consistent with the maximum lag examined. A 95% confidence interval for PEI was estimated by event-level bootstrap: the set of $n_{met}$ meteorological onset times was resampled with replacement 500 times, and PEI was recomputed for each replicate against the original fixed hydrological onset set; the 2.5th and 97.5th percentiles defined the interval bounds. Fixing the hydrological onset set isolates uncertainty in the meteorological precursor count; this causes the CI to understate total uncertainty when $n_{hyd}$ is also small, a limitation noted where relevant in the Results. The lag to the first matching SLLI onset within each matched pair was additionally recorded; distributions are summarised as median and mean propagation lag.

#### *2.6.3. Attribution model*

An OLS regression model with Newey–West HAC standard errors was used to partition SLLI variance between the dominant meteorological driver at its optimal lag and LULC change. Annual LULC variables were compressed into principal components (PCA; 85% cumulative variance threshold) before model entry to mitigate multicollinearity. Full model specification, cross-validation diagnostics, and Granger causality analysis are given in Supplementary Section S1.10-S1.11.

## 3. Results

### 3.1. Climatic trends in precipitation and evaporative demand

Over the 44-year study period (1981–2024) (Figure 2), mean annual precipitation (PCP) was 746.7 ± 143.6 mm at İznik and 741.1 ± 151.2 mm at Uluabat. Both records exhibit high interannual variability (coefficients of variation of 19% and 20%, respectively) but no statistically significant directional trend, as confirmed by the Mann-Kendall test (İznik: $\tau = -0.030$, $p = 0.785$; Uluabat: $\tau = -0.061$, $p = 0.564$). Sen's slope estimates of −0.68 and −0.87 mm yr$^{-1}$ correspond to non-significant long-term losses of approximately 6.8 and 8.7 mm per decade, respectively. Seasonal decomposition revealed no significant trend in PCP during any of the four seasons at either lake Table 3, although autumn (SON) showed the

steepest, albeit non-significant, negative slopes (−1.22 mm $yr^{-1}$ at İznik; −0.93 mm $yr^{-1}$ at Uluabat), consistent with a regional drying tendency in the transition season previously reported for western Anatolia.

Potential evapotranspiration (PET) told a starkly different story. Mean annual PET was 865.3 ± 50.7 mm at İznik and 992.2 ± 59.6 mm at Uluabat, both exceeding mean annual PCP and thus placing both catchments in a state of chronic annual water deficit. More critically, PET exhibited a highly significant monotonic increase at both stations (İznik: $\tau = 0.579$, $p < 0.001$; Uluabat: $\tau = 0.533$, $p < 0.001$), with Sen's slopes of +2.90 and +3.35 mm $yr^{-1}$, equivalent to gains of approximately +29 and +34 mm per decade, respectively. Integrated across the study period, these rates imply cumulative PET increases of roughly +125 mm at İznik and +145 mm at Uluabat between 1981 and 2024, a rise of around 15% and 14% above baseline values. The sub-period analysis further illustrates this shift: mean annual PET rose from 817 mm (İznik) and 943 mm (Uluabat) in the 1981–1990 decade to 905 mm and 1039 mm in the 2011–2024 period, respectively (Table 3).

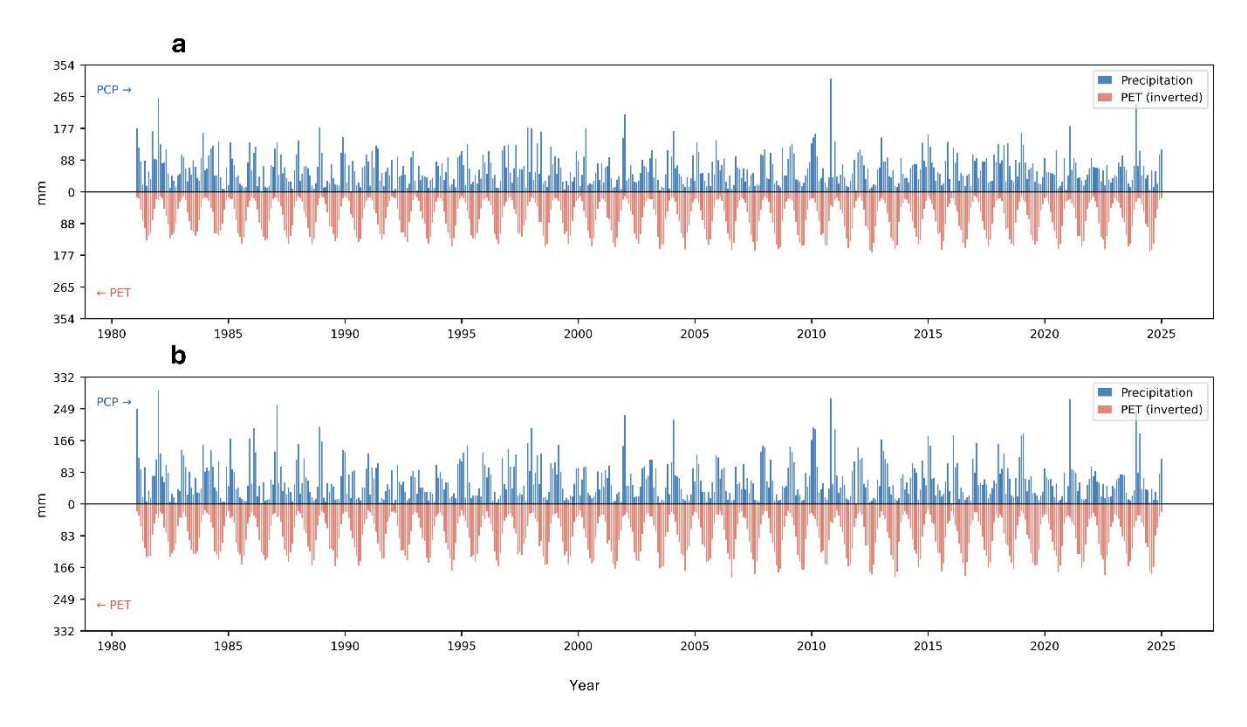


*Figure 2. Time series of monthly total PCP and PET values for the study area during the analysis period for basins Iznik (a) and Uluabat (b).*

Seasonally, the PET increase was significant across all four seasons at both lakes (Table 3). The dominant contribution came from summer (JJA), with Sen's slopes of +1.63 mm $yr^{-1}$ at İznik and +1.88 mm $yr^{-1}$ at Uluabat (both $p < 0.001$), reflecting amplified atmospheric evaporative demand during the driest months of the year. Significant but smaller PET increases were also detected in winter (DJF; $p < 0.001$ at both lakes), spring (MAM; $p = 0.007$ and $p = 0.049$), and autumn (SON; $p = 0.005$ and $p = 0.016$), indicating a thermally driven intensification of evaporative demand across all seasons rather than a single-season warming signal.

Taken together, the absence of any significant PCP trend alongside a robust, multi-seasonal PET increase has progressively widened the climatological water deficit at both lake basins. This asymmetric change, stable supply, rising demand, provides the direct climatic mechanism underpinning the post-2000 divergence between SPI and SPEI documented in Section 3.2.3, and has direct implications for the long-term water balance of both lakes.

*Table 3. Mann-Kendall trend test statistics and Sen's slopes for Annual and seasonal PCP and PET at İznik and Uluabat lakes, 1981–2024. Bold indicates statistical significance ($p < 0.05$).*

| Period/ Season | İznik PCP | | İznik PET | | Uluabat PCP | | Uluabat PET | |
|---|---|---|---|---|---|---|---|---|
| | **mean ± SD (CV%)** | | **mean ± SD (CV%)** | | **mean ± SD (CV%)** | | **mean ± SD (CV%)** | |
| Annual | 746.7 ± 143.6 (19.2%) | | 865.3 ± 50.7 (5.9%) | | 741.1 ± 151.2 (20.4%) | | 992.2 ± 59.6 (6.0%) | |
| | Slope (mm/yr) | *p* | Slope (mm/yr) | *p* | Slope (mm/yr) | *p* | Slope (mm/yr) | *p* |
| Annual | −0.68 | *0.785* | **+2.90** | ***<0.001*** | −0.87 | *0.564* | **+3.35** | ***<0.001*** |
| DJF | +0.16 | *0.864* | **+0.37** | ***<0.001*** | +0.51 | *0.739* | +0.40 | *0.003* |
| MAM | −0.01 | *0.992* | +0.55 | *0.007* | −0.53 | *0.473* | +0.46 | *0.049* |
| JJA | +0.31 | *0.448* | **+1.63** | ***<0.001*** | +0.19 | *0.664* | **+1.88** | ***<0.001*** |
| SON | −1.22 | *0.206* | +0.41 | *0.005* | −0.93 | *0.229* | +0.50 | *0.016* |

## 3.2. Meteorological drought characterization

### *3.2.1. Drought frequency and severity*

Table 4 and Figure 3 present the frequency of drought categories at each timescale for both lakes. At the 12-month scale, the most hydrologically relevant for lake water balance, dry conditions (SPI/SPEI < −1.0) occurred in approximately 15–17% of months at both sites, broadly consistent with theoretical expectations under a standard normal distribution (~15.9%). Extreme drought events (index < −2.0) were somewhat more frequent than expected at the 12-month scale, accounting for 3.3% (İznik SPI-12) and 2.3–2.5% (Uluabat) of all months, compared with the theoretical 2.3%. The most extreme monthly values recorded were SPI-12 = −2.82 at İznik (November 1993) and SPI-12 = −2.47 at Uluabat (January 2023), indicating at least two distinct extreme drought regimes separated by three decades.

*Table 4. Drought frequency by class (% of months) for SPI and SPEI at 12-month accumulation, İznik and Uluabat lakes, 1981–2024.*

| Lake | Index | Moderate dry (−1.5 to −1.0) | Severe dry (−2.0 to −1.5) | Extreme dry (< −2.0) | All dry (< −1.0) | Min value |
|---|---|---|---|---|---|---|
| İznik | SPI-12 | 8.9% | 3.3% | 3.3% | 15.5% | −2.82 |
| İznik | SPEI-12 | 9.3% | 4.3% | 3.1% | 16.6% | −2.44 |
| Uluabat | SPI-12 | 8.1% | 5.6% | 2.3% | 16.1% | −2.51 |

| | | | | | | |
|---|---|---|---|---|---|---|
| Uluabat | SPEI-12 | 11.6% | 3.5% | 2.5% | 17.6% | −2.55 |

### *3.2.2. Major drought episodes*

The 44-year record reveals several climatologically distinct drought episodes (Figure 3). The most severe and sustained dry period of the pre-2000 era occurred between mid-1992 and early 1994, when SPI-12 remained below −1.5 for approximately 18 consecutive months at İznik (minimum −2.82, November 1993) and for roughly 14 months at Uluabat (minimum −2.51, November 1993). A second notable episode centred on 2007, where İznik experienced extreme hydroclimatic drought under both indices simultaneously (SPI-12 = −2.34, SPEI-12 = −2.39 in spring–summer 2007), while Uluabat showed more moderate SPI-12 values (below −1.6) but pronounced SPEI-12 anomalies. A further severe drought emerged in 2013–2014, detectable primarily in SPEI-12 at both lakes, with İznik SPEI-12 reaching −2.44 in March 2014 despite comparatively moderate SPI-12 values (−2.03 in February 2014).

The most recent drought phase (2020–2023) was the most prolonged in the Uluabat record, with SPI-12 and SPEI-12 remaining below −1.5 for over 15 consecutive months, peaking at SPI-12 = −2.47 and SPEI-12 = −2.55 in January 2023 and May 2020, respectively. At İznik, this episode was comparatively less severe in SPI-12 but similarly pronounced in SPEI-12, reinforcing a pattern of amplified evapotranspiration-driven moisture deficits in the most recent period.

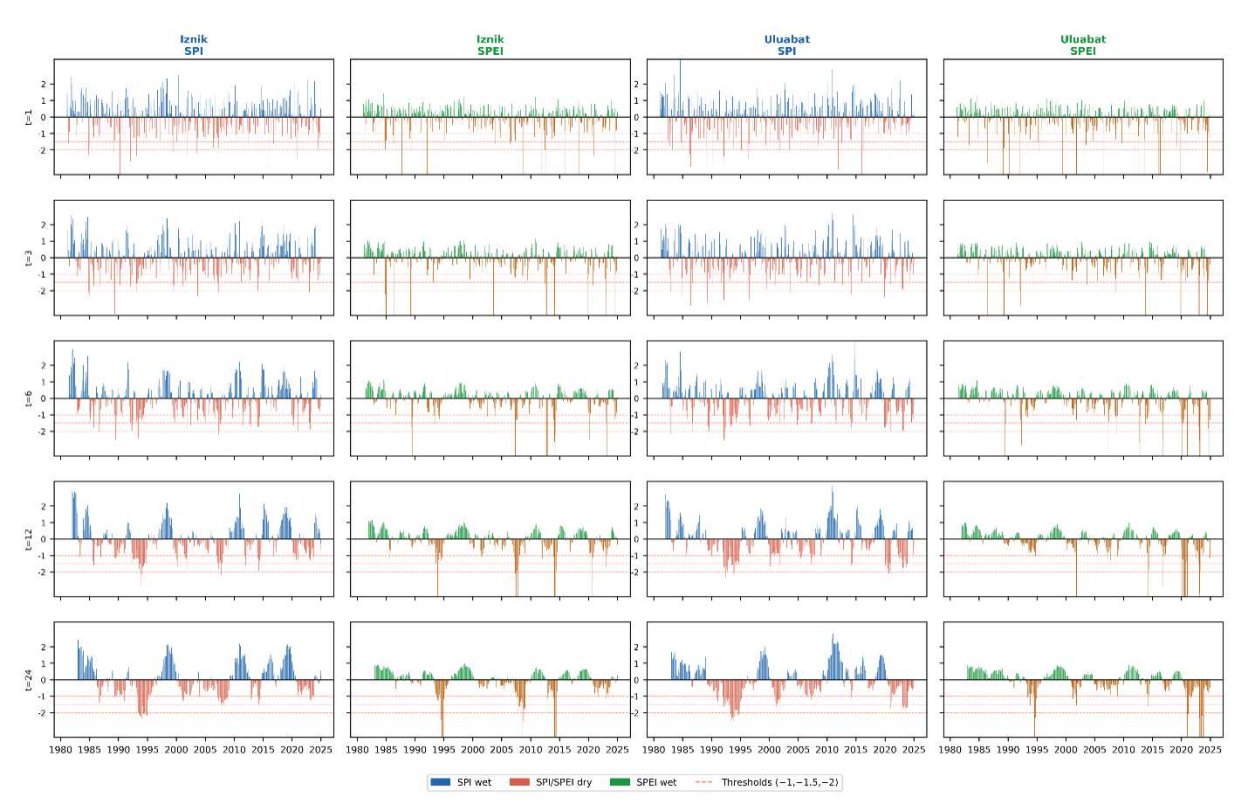


*Figure 3. Comparative time-series graphs of SPI and SPEI for the study period, shown on different time scales.*

#### *3.2.3. SPI–SPEI divergence and the role of evaporative demand*

A systematic divergence between SPI and SPEI emerged across both lakes at longer timescales and was consistent in direction (Table 5). During the 1980s and 1990s, SPEI-12 was on average 0.24–0.36 units higher (wetter) than SPI-12, suggesting that PET at the time was insufficient to create additional water stress beyond that implied by precipitation deficits alone. This relationship reversed from the 2000s onward: SPEI-12 was consistently 0.13–0.31 units more negative than SPI-12, particularly in the 2010s and 2020s. The practical consequence is stark: comparing the two sub-periods 1981–2000 and 2001–2024, SPI-12 drought frequency at İznik was essentially unchanged (18.3% vs. 13.2%), while SPEI-12 drought frequency more than doubled (9.6% to 22.2%). The same pattern holds at Uluabat, where SPI-12 drought frequency was stable at ~16% across both periods, but SPEI-12 drought frequency rose from 7.9% to 25.3%. These results indicate that rising atmospheric evaporative demand, not precipitation reduction per se, is the primary driver of intensifying drought conditions at both lakes in the post-2000 period.

*Table 5. Decadal mean SPI-12, SPEI-12, and their difference (SPEI-12 − SPI-12) at İznik and Uluabat lakes.*

| Decade | İznik SPI-12 | İznik SPEI-12 | Difference | Uluabat SPI-12 | Uluabat SPEI-12 | Difference |
|---|---|---|---|---|---|---|
| 1980s | +0.237 | +0.497 | +0.260 | +0.450 | +0.688 | +0.238 |
| 1990s | −0.181 | +0.138 | +0.320 | −0.287 | +0.071 | +0.358 |
| 2000s | −0.322 | −0.454 | −0.133 | −0.274 | −0.379 | −0.105 |
| 2010s | +0.455 | +0.161 | −0.294 | +0.525 | +0.216 | −0.309 |
| 2020s | −0.283 | −0.551 | −0.268 | −0.638 | −0.946 | −0.307 |

### 3.3. Hydrological drought assessment

#### *3.3.1. Composite series quality and SLLI robustness*

For both Lake İznik and Lake Uluabat, the bias-corrected composite lake level series spans 384 months (January 1993–December 2024), yielding a continuous record that significantly pre-dates the availability of in-situ gauge observations at either site (Table S2). For Lake İznik, in-situ gauge data were available for 268 months (January 2000–September 2024), providing the primary calibration window; satellite altimetry (ESA/CryoSat-2-based) covered the full 384-month period, and DAHITI altimetric records contributed an additional 104 months of overlapping coverage (May 2016–December 2024). The composite series was therefore anchored to the gauge during the observed period and extended retrospectively and prospectively using only altimetric sources. For the months without in-situ data (January 1993–December 1999 and October 2024–December 2024), the composite relies exclusively on satellite altimetry, which carries the higher source weight for İznik ($w_{Sat}$ = 0.717, $w_{DAHITI}$ = 0.283; see Section S2.2 and Table S2).

For Lake Uluabat, gauge data spanned October 2003–September 2024 (N = 245 months), with satellite altimetry again covering the full 384-month record and DAHITI contributing 102 months (May 2016–December 2024). Notably, the source weights at Uluabat were near-equal and reversed relative to İznik: the DAHITI product received slightly higher weighting ($w_{Sat}$ = 0.452, $w_{DAHITI}$ = 0.548), reflecting the comparatively closer agreement between DAHITI altimetry and the gauge record at this site during the overlapping period (Table S2).

### 3.3.2. SLLI time series and drought event characterization

The SLLI demonstrated high structural stability across empirical (Table 7), gamma, log-normal, and Weibull distribution fits, though parametric variants exhibited a slight over-detection bias compared to the empirical benchmark. Furthermore, leave-one-out (LOO) stability analysis confirmed the index is highly robust, perfectly preserving rank order and ruling out the presence of unduly influential outliers.

Application of the empirical SLLI revealed fundamentally different drought typologies between the two basins. Lake İznik's record was overwhelmingly dominated by a single, highly severe 37-month episode from 2020 to 2023, making its event identification highly sensitive to threshold selection. Conversely, Lake Uluabat experienced more frequent, shorter, and temporally distributed drought events, resulting in a much more gradual threshold sensitivity (Table 6). Comprehensive parametric cross-correlations, LOO stability metrics, and detailed event histories are provided in Table 6 and Table 7 and the Supplementary Material (Tables S3–S5).

*Table 6. Drought events identified from the empirical SLLI at the SLLI ≤ −1.0 threshold for both lakes (January 1993–December 2024). Major events (duration ≥ 9 months) are explicitly listed; lower-intensity Uluabat events are aggregated (see Table S7 for the complete 13-event breakdown).*

| Lake | Start | End | Duration (months) | Min. SLLI | Mean SLLI | Severity |
|---|---|---|---|---|---|---|
| **İznik** | Oct 2009 | Dec 2009 | 3 | −1.097 | −0.757 | 2.27 |
| | Dec 2019 | Jun 2020 | 7 | −1.097 | −1.078 | 7.55 |
| | **Oct 2020** | **Oct 2023** | **37** | **−1.691** | **−1.444** | **53.44** |
| | Jun 2024 | Oct 2024 | 5 | −1.097 | −1.008 | 5.04 |
| **Uluabat** | **Dec 2006** | **Dec 2007** | **13** | **−1.691** | **−1.533** | **19.93** |
| | May 2008 | Jan 2009 | 9 | −1.691 | −1.302 | 11.72 |

*Severity is defined as the absolute sum of negative SLLI values over the event duration. Bold denotes the most severe event per lake.*

*Table 7. SLLI class frequency distribution over the full 384-month composite record for both lakes, based on the empirical transformation.*

| Drought Class | SLLI Range | İznik (N) | İznik (%) | Uluabat (N) | Uluabat (%) |
|---|---|---|---|---|---|
| Extremely wet | > 1.645 | 12 | 3.1 | 12 | 3.1 |
| Very wet | 1.282–1.645 | 12 | 3.1 | 13 | 3.4 |
| Moderately wet | 0.842–1.282 | 38 | 9.9 | 35 | 9.1 |
| Near normal | −0.842–0.842 | 274 | 71.4 | 276 | 71.9 |
| Moderate drought | −1.282 to −0.842 | 36 | 9.4 | 36 | 9.4 |
| Severe drought | −1.645 to −1.282 | 12 | 3.1 | 12 | 3.1 |
| Extreme drought | < −1.645 | 0 | 0.0 | 0 | 0.0 |

*The maximum empirical SLLI magnitude of ±1.691 in both lakes reflects the constraint imposed by 384 available observations.*

### 3.3.3. *SLLI validation against SNDWI*

SLLI cross-validation against SNDWI (Figure 4 and Figure 5 and Table 8) revealed a significant ordinal relationship for Lake İznik but failed entirely for Lake Uluabat, where shallow depths, high turbidity, and seasonal macrophyte dynamics inverted the expected volume-reflectance relationship (F1 = 0.000). This stark divergence demonstrates that satellite-derived surface-extent proxies are fundamentally invalid for tracking drought signals in optically complex, vegetation-rich basins, with comprehensive cross-lag statistics detailed in Supplementary Table S6.

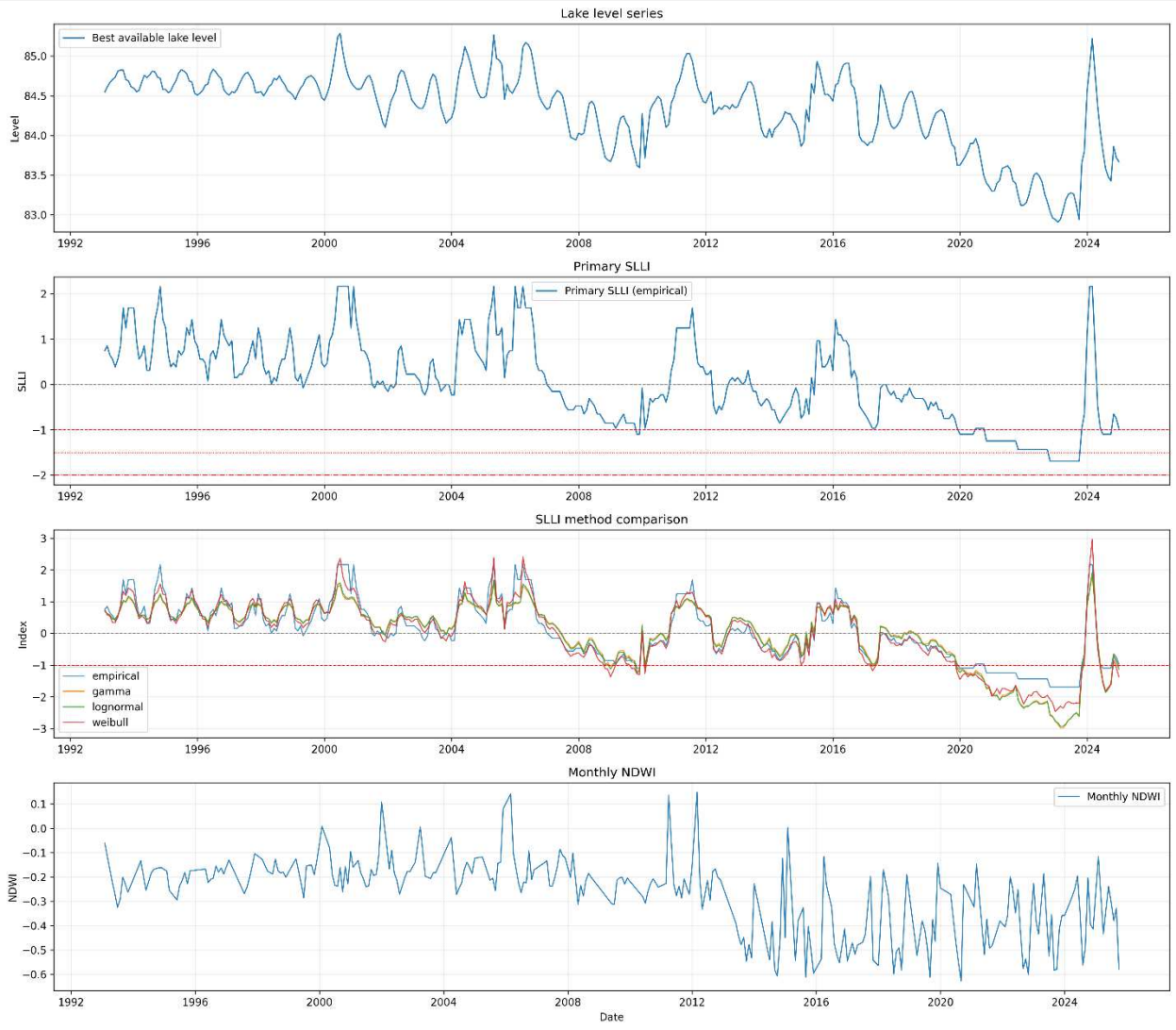


*Figure 4. Robustness assessment of the SLLI for Lake Iznik.* ***(a)*** *Monthly lake level time series from the best-available source.* ***(b)*** *Primary SLLI (empirical distribution); dashed lines mark moderate (SLLI < −1) and severe (SLLI < −2) drought thresholds.* ***(c)*** *SLLI sensitivity to probability distribution choice (empirical, gamma, log-normal, Weibull).* ***(d)*** *Satellite-derived monthly NDWI.*

*Table 8. Cross-validation statistics for the SLLI–SNDWI comparison for both lakes.*

| Statistic | Lake İznik | Lake Uluabat |
|---|---|---|

| | | |
|---|---|---|
| N (concurrent observations) | 263 | 184 |
| Pearson r (lag 0) | 0.451*** | −0.130 (n.s.) |
| Pearson p-value | $1.3 \times 10^{-14}$ | 0.079 |
| Spearman ρ (lag 0) | 0.487*** | −0.138 (n.s.) |
| Spearman p-value | $5.1 \times 10^{-17}$ | 0.062 |
| Best lag (months) | 3 | 12 |
| Best-lag r | 0.478 | −0.265** |
| Categorical accuracy | 80.9% | 78.8% |
| Cohen's κ | 0.134 | −0.114 |
| Multi-class F1 | 0.242 | 0.000 |

*n.s. = not significant (α = 0.05). ** p < 0.01. *** p < 0.001. The negative κ at Uluabat indicates categorical agreement below chance level.*

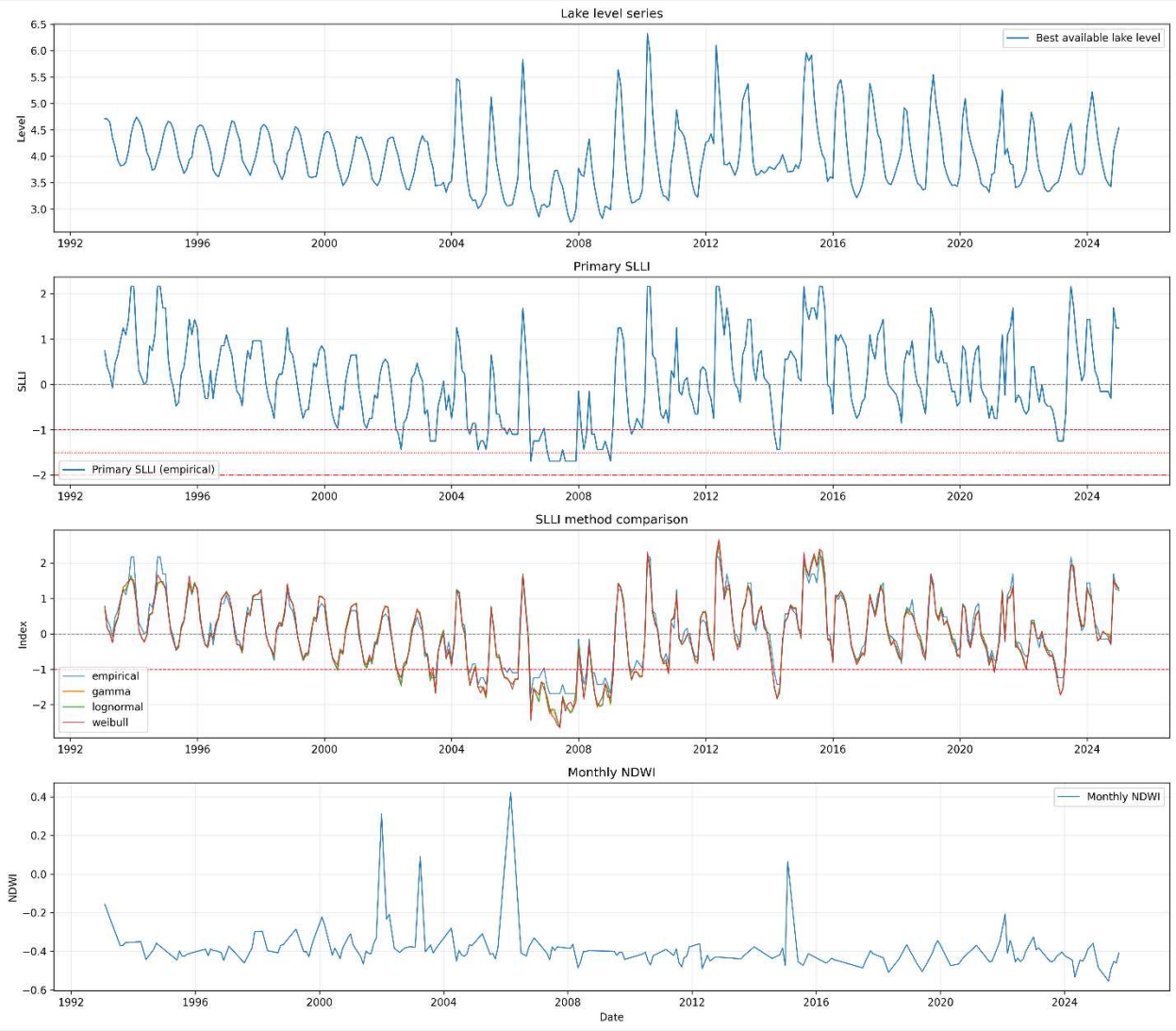


*Figure 5. Robustness assessment of the SLLI for Lake Uluabat. **(a)** Monthly lake level time series from the best-available source. **(b)** Primary SLLI (empirical distribution); dashed lines mark moderate (SLLI <*

*−1) and severe (SLLI < −2) drought thresholds.* ***(c)*** *SLLI sensitivity to probability distribution choice (empirical, gamma, log-normal, Weibull).* ***(d)*** *Satellite-derived monthly NDWI.*

### 3.4. Drought propagation analysis

#### *3.4.1. Lagged cross-correlation*

Despite sharing a common observational period (January 1993–December 2024; n = 384 months) and an identical analytical framework, SPI and SPEI at accumulation periods of 1, 3, 6, 12, and 24 months evaluated against the SLLI across lags of 0–24 months, the two lakes exhibit fundamentally different patterns of meteorological–hydrological drought coupling (Figure 6 and Figure 7 and Table 9).

At Lake Uluabat, statistically significant positive cross-correlations were identified at accumulation periods of 1–6 months and lags of 0–3 months (all *p*eff ≤ 0.034). The two strongest couplings were SPEI-3 at lag 1 (r = 0.326, *n*eff = 162, 95% CI [0.181, 0.457]) and SPEI-6 at lag 0 (r = 0.315, *n*eff = 114, 95% CI [0.140, 0.472]). Across all accumulation periods, SPEI consistently produced larger correlations than the corresponding SPI; for instance, SPEI-3 vs. SPI-3 at lag 1: r = 0.326 vs. 0.298, an asymmetry attributable to the incorporation of PET in SPEI formulations under Mediterranean warm-season water stress. No significant correlation was detected for the 12- or 24-month indices at any tested lag, delimiting the hydrological response window at Uluabat to sub-annual timescales and precluding long-memory coupling of the kind characteristic of deeper or more isolated basins.

At Lake İznik, no statistically significant cross-correlation was identified at any index, timescale, or lag at the 5% or 10% significance level (minimum *p*eff = 0.155; Table 9). This result does not imply the absence of physical coupling; rather, it reflects the inferential constraint imposed by the pronounced serial persistence of the İznik SLLI (lag-1 autocorrelation: r(1) = 0.927), which reduces effective sample sizes from n = 384 to *n*eff ≈ 24–28 at the 24-month accumulation period (a 93% reduction) and to *n*eff ≈ 40–43 at the 12-month period. Under these conditions, detection of significance at α = 0.05 would require $|r| \gtrsim 0.40–0.50$; a threshold the observed correlations do not approach. Directionally, SPEI again outperformed SPI at every accumulation period, with the highest point estimates at SPEI-12/lag-1 (r = 0.196; 95% CI [−0.114, 0.471]) and SPEI-24/lag-1 (r = 0.194; 95% CI [−0.197, 0.531]), consistent with long-timescale PET-modulated forcing that the record length cannot resolve statistically.

The cross-correlation contrast between the two lakes is therefore not merely one of magnitude but of structural character. Uluabat behaves as a short-memory, flow-through system in which precipitation and evapotranspiration anomalies at seasonal scales (1–6 months) propagate detectably to lake levels within 0–3 months. İznik, as a closed-basin lake with multi-year level inertia, integrates forcing over much longer timescales, physically consistent with 12-month-scale meteorological antecedents, but its propagation dynamics are statistically inaccessible from the 32-year record alone.

*Table 9. Comparative peak lagged cross-correlations between meteorological drought indices and the SLLI for both lakes (January 1993–December 2024; n = 384). Peak r is the maximum absolute correlation over lags 0–24 months. Statistical significance is assessed using neff-adjusted p-values (peff). Bold entries indicate significance at α = 0.05.*

| Index | İznik: Peak r (lag) | İznik peff | İznik neff | Uluabat: Peak r (lag) | Uluabat peff | Uluabat neff | Sig.† |
|---|---|---|---|---|---|---|---|

| | | | | | | | |
|---|---|---|---|---|---|---|---|
| SPI-1 | −0.077 (lag 0) | 0.165 | 325 | +0.179 (lag 1) | **<0.001** | 383 | ✓ |
| SPEI-1 | +0.075 (lag 8) | 0.179 | 326 | +0.221 (lag 1) | **<0.001** | 359 | ✓ |
| SPI-3 | −0.068 (lag 20) | 0.454 | 122 | +0.298 (lag 1) | **<0.001** | 185 | ✓ |
| SPEI-3 | +0.125 (lag 1) | 0.155 | 130 | +0.326 (lag 1) | **<0.001** | 162 | ✓ |
| SPI-6 | +0.058 (lag 2) | 0.622 | 75 | +0.263 (lag 0) | 0.002 | 132 | ✓ |
| SPEI-6 | +0.165 (lag 2) | 0.176 | 68 | +0.315 (lag 0) | 0.001 | 114 | ✓ |
| SPI-12 | −0.047 (lag 12) | 0.772 | 41 | ≤+0.148 | >0.18 | 84 | — |
| SPEI-12 | +0.196 (lag 1) | 0.212 | 42 | +0.177 (lag 0) | 0.106 | 84 | — |
| SPI-24 | −0.130 (lag 24) | 0.543 | 24 | ≤+0.148 | >0.18 | 49 | — |
| SPEI-24 | +0.194 (lag 1) | 0.328 | 28 | +0.136 (lag 0) | 0.327 | 54 | — |

*Notes: r, Pearson cross-correlation coefficient; peff, two-tailed p-value based on neff; neff, effective sample size corrected for serial autocorrelation (Chelton, 1983 for İznik; Quenouille, 1952 Quenouille, 1952 for Uluabat). Bold entries indicate peff < 0.05. †Significance column refers to Lake Uluabat only; no İznik value achieved significance.*

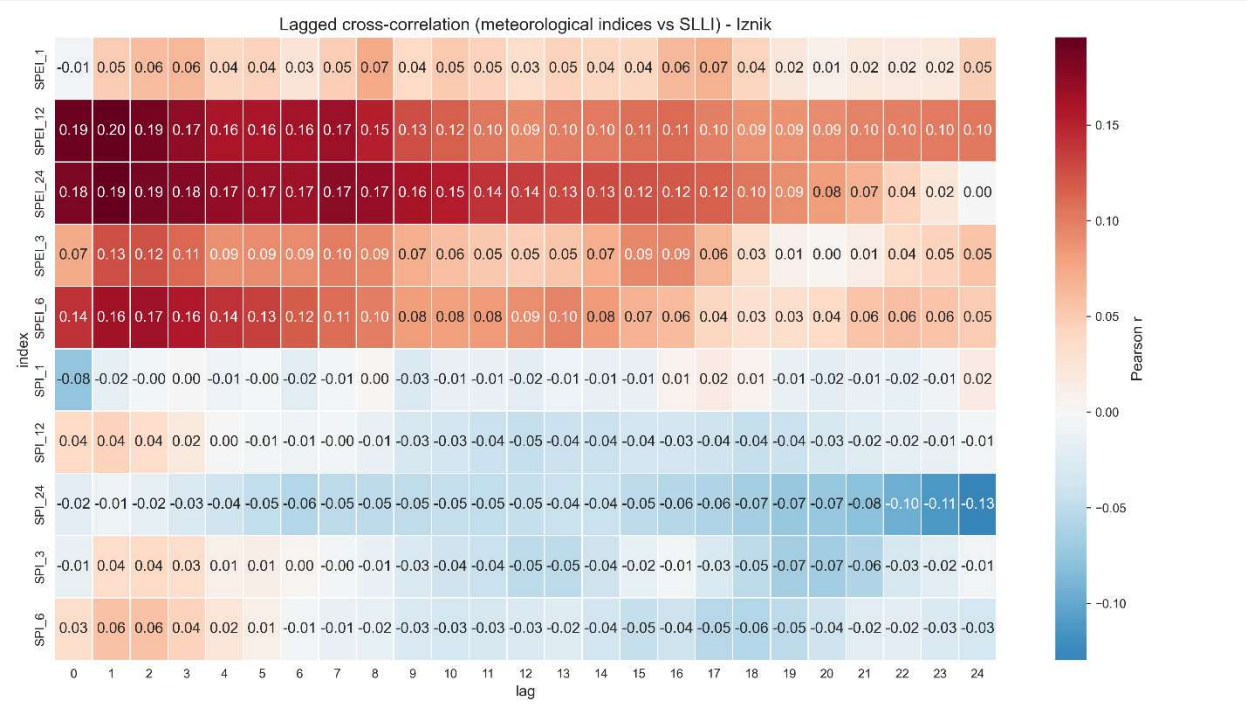


*Figure 6. Lagged cross-correlation heatmap between SPI and SPEI (1-, 3-, 6-, 12-, and 24-month timescales) and the SLLI for Lake İznik, at lags 0–24 months.*

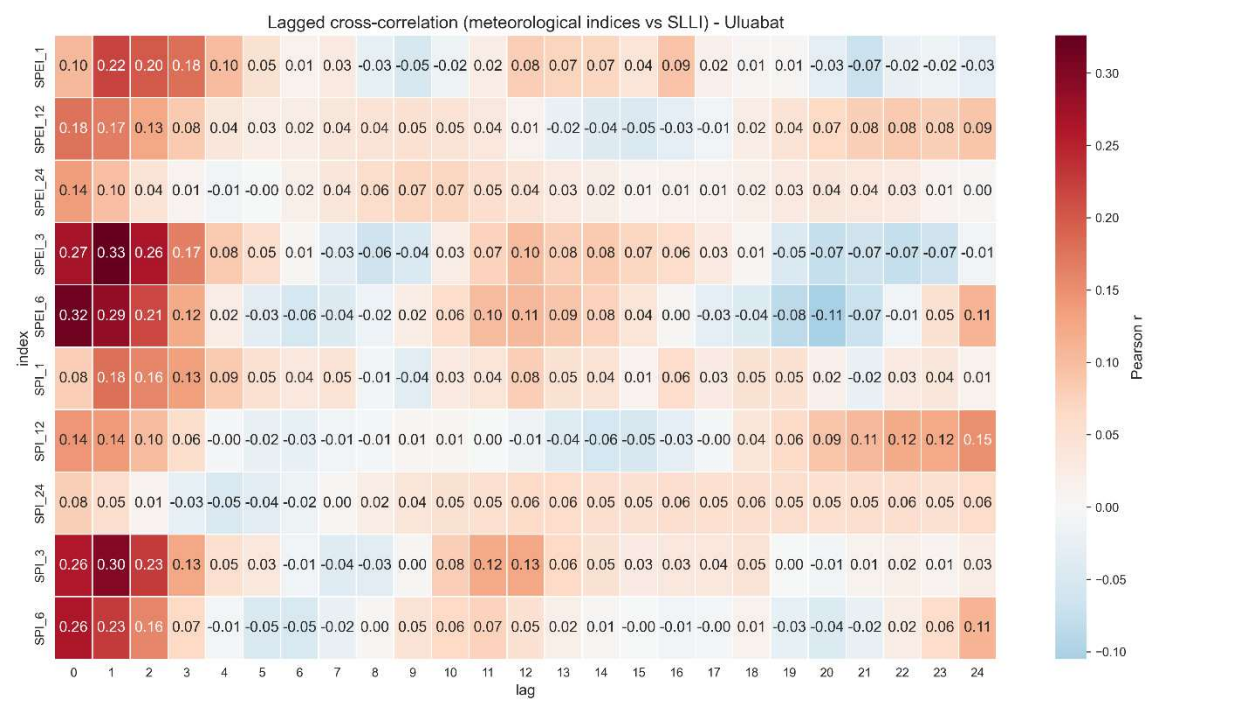


*Figure 7.Lagged cross-correlation heatmap between SPI and SPEI (1-, 3-, 6-, 12-, and 24-month timescales) and the SLLI for Lake Uluabat, at lags 0–24 months.*

### *3.4.2. Event-based propagation*

Event-based analysis reveals a sharp contrast in drought occurrence frequency, duration, and propagation dynamics between the two lakes (Table 10). Over the common 32-year record, 13 discrete hydrological drought events were identified at Lake Uluabat versus only 4 at Lake İznik, reflecting fundamental differences in basin hydrological memory and meteorological sensitivity.

At Lake İznik, the four events display pronounced asymmetry in duration and severity: a single episode spanning October 2020 to October 2023 (37 months) accounted for 71% of all drought months and approximately 80% of cumulative severity (52.5 of 65.6 SLLI-units). The three remaining events (durations of 2, 6, and 4 months) barely exceeded the −1.0 threshold, reflecting transient responses to sub-seasonal precipitation deficits rather than sustained hydrological drought. The dominant 2020–2023 event was preceded by a severe SPEI-12 episode beginning in January 2020 (SPEI-12 = −1.255 at onset; minimum −2.197 in August 2020), with a propagation lag of approximately 9–10 months from the 12-month meteorological drought onset to the sustained hydrological drought onset, consistent with the basin-response timescale of a closed-water-body system receiving catchment runoff and direct precipitation under semi-arid conditions. Brief events (durations ≤ 6 months) exhibited propagation lags of approximately one month from SPEI-6 onset, though their shallow threshold exceedances preclude robust lag estimation. Throughout, sustained hydrological drought at İznik required concurrent, multi-timescale meteorological deficits, particularly persistent negative SPEI-12 and, for the dominant event, ultimately SPEI-24 crossing into drought territory, rather than episodic sub-seasonal anomalies alone.

At Lake Uluabat, the 13 events range in duration from 1 to 12 months, with the longest and most severe episode spanning December 2006 to December 2007 (13 months; mean SLLI = −1.533). Seven of

the 13 events cluster within the 2004–2009 period, during which the most severe sustained meteorological droughts on record affected the region. Of 39 identified SPEI-3 meteorological drought events (SPEI-3 < −1.0), 13 propagated to SLLI < −1.0 within a 6-month forward window (propagation rate: 33.3%; bootstrap 95% CI [15.4%, 48.7%]; mean propagation lag: 1.8 months; 95% CI [1.0, 2.9] months). Four short-duration events (1 month each) occurred under neutral or positive contemporaneous SPEI-3, implicating non-meteorological forcing, most plausibly anthropogenic water abstractions from the Mustafakemalpaşa River, rather than drought propagation per se. The moderate overall propagation rate (31%) is consistent with substantial catchment buffering that limits meteorological-to-hydrological drought transmission to periods of sustained, rather than isolated, moisture deficits.

The event-based comparison thus reveals a dichotomy in propagation regime. İznik behaves as a slow-responding, integrative system with rare but prolonged drought events and long propagation lags (~9–10 months for the dominant episode), in which only multi-timescale atmospheric forcing produces sustained hydrological drought. Uluabat responds rapidly and frequently to seasonal moisture deficits, mean propagation lag ~2 months, but retains sufficient buffering capacity that only approximately one-third of antecedent meteorological drought events successfully propagate to the hydrological domain. Lake-specific event summaries are provided in Tables S10 and S11 (Supplementary).

In Uluabat lake, application of the PEI framework to the best-performing driver (SPEI-3) identified 13 meteorological drought onset events over the 1993–2024 analysis period, of which 4 were matched by an SLLI onset within 24 months, yielding PEI = 0.308 [95% bootstrap CI: 0.154–0.487]. The median propagation lag across matched events was 1.8 months [mean: 1.8 months], consistent with the cross-correlation peak at lag 1–2 months. The wide bootstrap confidence interval reflects the modest number of discrete events available for estimation over a 32-year record; PEI is therefore best interpreted as an order-of-magnitude characterisation of propagation fidelity rather than a precise efficiency estimate.

Only 4 meteorological drought onset events were detectable in the SPEI-12 series over the analysis period, reflecting the extreme scarcity of the multi-year atmospheric deficits required to perturb this high-storage system in Iznik lake. With $n_{met} = 4$, the event-level bootstrap produces a confidence interval spanning nearly the full [0, 1] range; PEI is therefore not reported for İznik. This outcome is itself informative: the rarity of propagated events is a direct manifestation of the basin's high hydrological memory and low propagation efficiency, and constitutes a qualitative PEI signal (near zero under current land-cover conditions) even in the absence of a precise numerical estimate.

*Table 10. Summary comparison of drought propagation characteristics between Lakes İznik and Uluabat (January 1993–December 2024). Propagation lag for İznik is based on the dominant Event 3 (2020–2023); propagation rate and mean lag for Uluabat are derived from event-bootstrap analysis of 39 SPEI-3 antecedent events.*

| Characteristic | Lake İznik | Lake Uluabat |
|---|---|---|
| SLLI lag-1 autocorrelation | 0.927 | Lower (near-stationary) |
| Number of SLLI drought events | 4 | 13 |
| Dominant event duration (months) | 37 (Oct 2020–Oct 2023) | 13 (Dec 2006–Dec 2007) |
| Total drought months | 52 | 61 |
| Minimum SLLI recorded | −1.691 | −1.691 |

| | | |
|---|---|---|
| Primary antecedent index | SPEI-12 | SPEI-3 / SPEI-6 |
| Propagation lag (dominant event) | ~9–10 months (from SPEI-12 onset) | Mean 1.8 months [95% CI: 1.0–2.9] |
| Propagation rate (% of met. events) | N/A (n = 4 events) | 30.8% [95% CI: 15.4–48.7%] |
| Events with non-meteorological forcing | 0 of 4 | ~4 of 13 (suspected) |

*Notes: Propagation lag and rate for Uluabat derived from case-resampling bootstrap (B = 500 replicates) on 39 identified SPEI-3 drought events. İznik propagation lag is a single-event estimate.*

*3.4.3. Attribution Models and Granger Causality*

Attribution analyses reinforce the propagation regime dichotomy identified above, while identifying distinct mechanisms and timescales of climatic control over lake-level variability at each site (Table 11 and Table 12).

For Lake Uluabat, a parsimonious two-predictor OLS model incorporating SPEI-3(t−1) and SPEI-6(t), the two index–lag combinations identified as physically interpretable and statistically robust in Section S3.6 (Supplementary), explained 12.2% of total SLLI variance ($R^2 = 0.122$; adjusted $R^2 = 0.118$; HAC F-statistic = 12.80; $p < 0.001$). Both predictors were statistically significant under Newey–West HAC-corrected inference (12-lag Bartlett kernel) to account for strong positive residual autocorrelation (Durbin–Watson = 0.44): SPEI-3(t−1), $\beta = 0.193$ (SEHAC = 0.051; $z = 3.79$; $p < 0.001$); SPEI-6(t), $\beta = 0.169$ (SEHAC = 0.071; $z = 2.39$; $p = 0.017$). The positive coefficients confirm that wetter antecedent conditions at seasonal-to-medium timescales correspond to elevated lake levels, as physically expected under a meteorological-to-hydrological drought propagation framework. The 87.8% of unexplained SLLI variance reflects primarily anthropogenic water abstractions from inflowing rivers and land-use-mediated changes in catchment water balance, structural factors external to the climate-only model, rather than model misspecification.

For Lake İznik, an unrestricted OLS model incorporating all ten contemporaneous SPI/SPEI indices yielded $R^2 = 0.306$ (adjusted $R^2 = 0.287$; $F(10, 373) = 16.43$; $p < 0.001$). Within this model, only the 24-month indices achieved nominal statistical significance, SPEI-24 ($\beta = +1.171$; $t = 6.47$; $p < 0.001$) and SPI-24 ($\beta = -1.149$; $t = -6.58$; $p < 0.001$), with opposing signs consistent with the extraction of the PET-sensitive moisture deficit component (SPEI minus SPI) as the dominant multi-year driver of lake-level variability. However, the Durbin–Watson statistic of 0.247 signals extreme positive residual autocorrelation, rendering conventional standard errors anti-conservative; HAC-corrected inference (Newey–West, truncation lag ≈ 9 months) is required before drawing firm conclusions from individual-predictor t-tests. In bivariate regressions, only SPEI-6, SPEI-12, and SPEI-24 achieved nominal significance ($R^2 = 0.020$, 0.037, and 0.034, respectively), confirming the weak contemporaneous linear coupling at monthly resolution and the dominance of the SPEI over SPI series in explaining month-to-month SLLI variance.

Granger causality tests provide the sharpest contrast between the two systems (Table 12). At Lake Uluabat, SPEI-3 Granger-caused SLLI at all tested lag orders from 1 to 12 months (F-statistics: 2.73–14.10; all $p \leq 0.006$), demonstrating consistent predictive temporal precedence from seasonal meteorological drought to hydrological drought across the full range of physically relevant timescales. This finding was robust to non-parametric resampling and confirms the cross-correlation and attribution results. SPEI-6 exhibited significant Granger causality at lags 3–8 and 11–12 ($p \leq 0.047$), becoming predictive only after

sufficient moisture accumulation. At Lake İznik, by contrast, Granger causality was restricted to the 12-month lag window: both SPI-12 ($F(12, 358) = 1.982$; $p = 0.025$) and SPEI-12 ($F(12, 358) = 2.278$; $p = 0.009$) significantly preceded SLLI at lag $p = 12$ months, with no shorter lag window yielding significance. Bootstrap-corrected p-values (MBB block length = 27 months; pboot = 0.031 and 0.044 for SPEI-12 and SPI-12 respectively) confirmed the robustness of these results. The combined Granger and event-based evidence thus converges on a characteristic predictive horizon of approximately 9–12 months for İznik versus 1–2 months for Uluabat, a near order-of-magnitude difference in propagation timescale attributable principally to their contrasting hydraulic architectures.

*Table 11. Attribution model summary for Lakes İznik and Uluabat. All models regress SLLI on contemporaneous (lag-0) or lagged SPI/SPEI predictors by OLS. Residual autocorrelation diagnostics and HAC correction status are noted.*

| Parameter | Lake İznik | Lake Uluabat |
|---|---|---|
| Predictors | All 10 SPI/SPEI indices (lag 0) | SPEI-3(t−1) + SPEI-6(t) |
| $R^2$ | 0.306 | 0.122 |
| Adjusted $R^2$ | 0.287 | 0.118 |
| F-statistic | 16.43 ($p < 0.001$) | 12.80 ($p < 0.001$) |
| Durbin–Watson | 0.247 (severe autocorrelation) | 0.44 |
| HAC correction applied? | No (required; see S3.6) | Yes (12-lag Bartlett kernel) |
| Nominally significant predictors | SPEI-24 (β = +1.171), SPI-24 (β = −1.149) | SPEI-3 (β = +0.193), SPEI-6 (β = +0.169) |
| Dominant timescale | 24 months (PET-modulated multi-year deficit) | 3–6 months (seasonal moisture balance) |
| Unexplained variance drivers | Long-memory basin dynamics; limited neff | Anthropogenic abstractions; LULC changes |

*Notes: β, OLS regression coefficient; HAC, heteroskedasticity- and autocorrelation-consistent (Newey–West); LULC, land use/land cover. The opposing signs of SPI-24 and SPEI-24 at İznik reflect the partial extraction of the PET component (SPEI minus SPI).*

*Table 12. Granger causality test results for selected meteorological indices predicting SLLI, at lag windows p = 1–12 months. Entries are F (p-value).*

| Index | Lake | Lag p = 1 | Lag p = 3 | Lag p = 6 | Lag p = 9 | Lag p = 12 | Consistent? |
|---|---|---|---|---|---|---|---|
| SPEI-3 | Uluabat | 14.10 (<0.001) | 5.62 (0.001) | 3.73 (0.001) | 2.65 (0.006) | 2.73 (0.002) | Yes (all lags) |
| SPEI-3 | İznik | — | — | — | — | — | Not tested |
| SPEI-6 | Uluabat | 1.37 (0.243) | 2.81 (0.039) | 2.32 (0.033) | 1.64 (0.101) | 1.88 (0.035) | Lags 3–8, 11–12 |
| SPEI-6 | İznik | 2.77 (0.097) | 0.89 (0.444) | 1.10 (0.360) | — | 1.23 (0.263) | No |
| SPI-12 | İznik | 0.27 (0.604) | 1.27 (0.286) | 1.33 (0.243) | — | 1.98 (0.025) | Lag 12 only |
| SPEI-12 | İznik | 1.02 (0.313) | 0.83 (0.478) | 1.16 (0.330) | — | 2.28 (0.009) | Lag 12 only |

| | | | | | | | |
|---|---|---|---|---|---|---|---|
| SPEI-12 | Uluabat | — | — | — | — | — | Not significant (any lag) |

*Notes: F, F-statistic for block-F Granger causality test (H0: index does not Granger-cause SLLI). Degrees of freedom: F(p, n−2p−1). For İznik, bootstrapped p-values (MBB; B = 500; block length = 27 months) confirmed SPEI-12 results at lag 12 (pboot = 0.031).*

### 3.5. Land use/land cover dynamics and anthropogenic attribution

GLC_FCS30D-derived LULC time series (2000–2022) reveal contrasting patterns of landscape dynamics between the two basins (Figure 8). In the İznik Basin, the dominant change was a modest reduction in tree/forest cover from 616.6 km² (44.1%) to 579.7 km² (41.5%), accompanied by an expansion of cropland from 216.4 km² (15.5%) to 245.1 km² (17.5%) and built-up land from 26.6 km² (1.9%) to 35.0 km² (2.5%). Water surface area remained essentially stable, declining marginally from 301.8 km² (21.6%) to 300.5 km² (21.5%), and rangeland/shrub/grass area was similarly unchanged, at 233.2 km² (16.7%) and 234.0 km² (16.8%) in 2000 and 2022, respectively.

In contrast, the Uluabat Basin exhibited minimal overall land-cover change, with cropland remaining the dominant class and increasing slightly from 472.4 km² (48.2%) to 480.3 km² (49.0%). Tree/forest cover declined modestly from 248.1 km² (25.3%) to 230.8 km² (23.5%), while flooded vegetation increased from 28.3 km² (2.9%) to 32.0 km² (3.3%) and built-up land expanded from 21.2 km² (2.2%) to 25.2 km² (2.6%). Water surface area declined marginally from 117.8 km² (12.0%) to 115.8 km² (11.8%), while rangeland/shrub/grass area increased slightly from 92.3 km² (9.4%) to 95.9 km² (9.8%). Overall, the Uluabat Basin maintained a comparatively stable land-cover composition throughout the study period (Figure 8).

Mann–Kendall analysis of the SPEI-12 residual SLLI series confirms highly significant non-climatic negative trends in both basins ($p < 0.0001$). The Theil–Sen slope estimator yields a residual hydrological decline of $\hat{\beta} = -0.00646$ SLLI month$^{-1}$ (95% CI: −0.00741 to −0.00564) at Lake Iznik and $\hat{\beta} = -0.00717$ SLLI month$^{-1}$ (95% CI: −0.00777 to −0.00650) at Lake Uluabat. The overlapping confidence intervals indicate that the absolute rate of non-climatic hydrological deterioration is statistically comparable across both lakes. This finding does not undermine the attribution narrative, the operative mechanisms differ fundamentally, but it establishes that the human-induced pressure on the hydrological cycle is of comparable absolute intensity at both sites.

Partial correlation analysis further constrains the attribution at each lake. At Lake İznik, the baseline concurrent correlation between SPEI-12 and SLLI is r = 0.232 (95% CI: 0.195 to 0.379), which is statistically significant yet modest, indicating a partial but incomplete coupling of contemporaneous lake levels with the regional atmospheric moisture signal. After controlling for GLC_FCS30D-derived cropland area, the partial correlation rises to r = 0.289 (95% CI: 0.195 to 0.379). This increase identifies cropland area as a suppressor variable at İznik: the progressive agricultural expansion, from 216.4 km² (15.5%) in 2000 to 245.1 km² (17.5%) in 2022, introduces a growing irrigation abstraction demand that depresses lake inflows independently of climatic forcing, co-occurring alongside a net decline in tree/forest cover from 616.6 km² (44.1%) to 579.7 km² (41.5%). Together, these land-use trajectories impose a compounding non-climatic signal on the lake water balance that, when removed through cropland control, reveals a modestly stronger underlying climate–lake coupling than the bivariate correlation alone suggests. At Lake Uluabat, the baseline correlation (r = 0.176; 95% CI: 0.083 to 0.277)

is statistically significant and remains essentially unchanged at r = 0.182 (95% CI: 0.083 to 0.277) when cropland is controlled, consistent with the negligible land-cover trajectory of the dominant cropland class, expanding by only 7.9 km² over the 2000–2022 period, which confers insufficient covariance with SPEI-12 to function as a meaningful confound. The persistence of the climate–lake signal after cropland control therefore reflects the dominant role of direct river abstraction from the Mustafakemalpaşa River rather than agriculturally mediated climate–hydrology coupling.

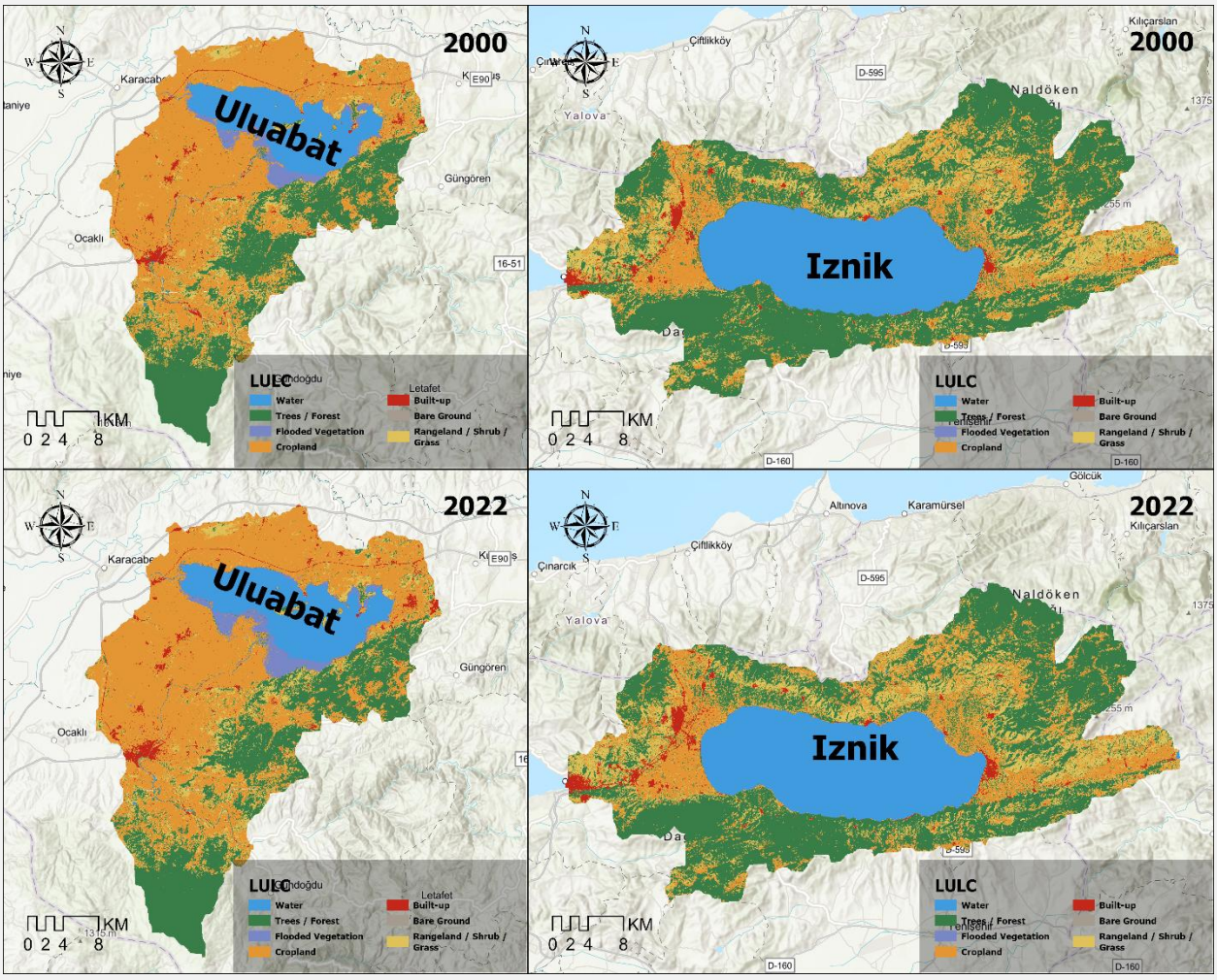


*Figure 8. Land use/land cover (LULC) classification maps for the Lake Uluabat (left) and Lake İznik (right) basins in 2000 (top) and 2022 (bottom), illustrating two decades of landscape change across both catchments.*

## 4. Discussion

### 4.1. Divergent propagation pathways: synthesis of the natural experiment

The central finding of this study, that two lakes separated by approximately 50 km, sharing virtually identical precipitation regimes and atmospheric evaporative demand, have followed fundamentally divergent hydrological drought trajectories over the period 1993–2024, provides compelling empirical support for the natural experiment design at the core of the analytical framework. At Lake Uluabat,

statistically significant meteorological-to-hydrological drought propagation operates on a seasonal timescale (SPEI-3/lag-1, r = 0.326; SPEI-6/lag-0, r = 0.315; Granger causality confirmed across all lag orders 1–12 months), with a mean propagation lag of 1.8 months [95% CI: 1.0–2.9] and a propagation efficiency of 30.8% of antecedent SPEI-3 drought events. At Lake İznik, no lagged cross-correlation achieved statistical significance at any index, timescale, or lag, and Granger causality was detectable only at a 12-month lag (SPEI-12: $F(12, 358) = 2.278$, $p = 0.009$; bootstrap-corrected $p_{boot} = 0.031$). Because both lakes experience essentially the same climatic forcing, this divergence cannot be attributed to differential precipitation or evaporative demand and must instead reflect differences in basin morphology, hydrological memory, and land cover. This interpretation is consistent with the theoretical framework of Van Loon et al. (2024), who characterise drought as a hydrological continuum in which basin-scale memory and connectivity govern the rate and fidelity of signal transfer across the terrestrial water cycle, and with the global synthesis of Xiong et al. (2025), who demonstrated across 1089 catchments that catchment baseflow index and topographic slope are among the strongest determinants of propagation characteristics at the event scale. Furthermore, Li et al. (2024) confirms that human regulation prolongs propagation time; LULC and cropland cover affect propagation direction and timing, which reinforce this research's natural experiment divergence finding.

### 4.2. The dominant role of evaporative demand in post-2000 drought intensification

The systematic divergence between SPI and SPEI documented in this study, a reversal from SPEI > SPI during the 1980s–1990s to SPEI < SPI from the 2000s onward, constitutes one of the study's most consequential findings. At Lake İznik, SPEI-12 drought frequency more than doubled between 1981–2000 and 2001–2024 (9.6% to 22.2%), while SPI-12 drought frequency was essentially unchanged (18.3% vs. 13.2%); the same pattern held at Lake Uluabat (SPEI-12: 7.9% to 25.3%; SPI-12: stable at ~16%). The mechanistic driver is unambiguous: GLEAM4-derived PET increased at highly significant rates at both lakes (İznik: +2.90 mm yr$^{-1}$, $\tau = 0.579$, $p < 0.001$; Uluabat: +3.35 mm yr$^{-1}$, $\tau = 0.533$, $p < 0.001$) across all four seasons, while annual precipitation exhibited no significant directional trend at either lake. These cumulative PET increases of approximately +125 mm (İznik) and +145 mm (Uluabat) between 1981 and 2024 place both basins in deepening chronic annual water deficit, a condition that is not captured by precipitation-only drought indices. This finding aligns directly with the global analysis of Gebrechorkos et al. (2025), who used satellite and reanalysis data to demonstrate that warming is the primary accelerant of drought severity globally, and with the attribution study of Bevacqua et al. (2024), which showed that evapotranspiration enhancement driven by antecedent warming accounted for 14–41% of the 2022 European drought's climate-change contribution. For seasonal drought prediction in the Mediterranean, Brands et al. (2025) underscore that SPEI systematically outperforms SPI in capturing multi-decadal aridity trends precisely because it integrates evaporative demand, a finding directly reproduced in our decadal SPEI–SPI difference analysis. In addition, Miao et al. (2026) documented that near-record 2025 warming substantially increased evaporative demand, triggering compound drought hotspots including the mediterranean and Mwinjuma et al. (2026) confirms that SPI and SPEI diverge most sharply in arid and semi-arid zones under warming climate.

The use of GLEAM4 (Amiri & Örüç, 2026; Miralles et al., 2025), which employs a Penman-based PET formulation calibrated against global eddy-covariance and sap flow observations, is central to resolving this signal. Temperature-only Thornthwaite-derived PET systematically underestimates demand under Mediterranean summer conditions (Sheffield et al., 2012; Vicente-Serrano et al., 2022); studies applying

Thornthwaite PET in this region will have underestimated both the magnitude of post-2000 drought intensification and its attribution to evaporative demand rather than precipitation deficit.

### 4.3. Basin architecture as the primary control on propagation regime

The near-order-of-magnitude difference in characteristic propagation timescale between the two lakes, approximately 9–10 months at İznik versus 1–2 months at Uluabat, reflects the interaction of three structural controls: basin depth and storage volume, catchment-to-lake area ratio, and hydrological connectivity. Lake İznik's deep tectonic morphology (maximum depth ~80 m; catchment: lake area ratio ~5.7) creates multi-year hydrological memory, evidenced by its SLLI lag-1 autocorrelation of 0.927. Under such conditions, a single month's precipitation or evapotranspiration anomaly contributes negligibly to the lake's integrated storage state; only sustained, multi-timescale atmospheric deficits, as demonstrated by the 37-month 2020–2023 drought event, which required concurrent negative SPEI-12 and ultimately SPEI-24 conditions to initiate, can drive a persistent hydrological drought response. This behaviour is analogous to, though more extreme than, the multi-year climate memory in shallow lake water levels documented by Leader et al. (2024) in Canadian Boreal systems, and is consistent with the closed-basin dynamics characterised by Baigaliyeva et al. (2024) for Shortandy Lake in Central Asia, where decadal-scale atmospheric forcing was required to explain observed lake-level trends. The severe effective sample size reduction imposed by İznik's SLLI persistence ($n_{eff} \approx 24$–$28$ at the 24-month accumulation scale; a 93% reduction from $n = 384$) means that the 32-year record is structurally insufficient to achieve statistical power for detecting the hypothesised 12–24 month coupling at $\alpha = 0.05$. The absence of significant cross-correlations at İznik should therefore be interpreted as a power limitation rather than as evidence against physical coupling, a distinction that Granger causality at lag 12 (confirmed by moving-block bootstrap) supports. Lake Uluabat's radically different architecture, extremely shallow (mean depth ~2 m), large catchment:lake area ratio (~40), and hydrological connectivity dominated by the Mustafakemalpaşa River, produces a fast-response, flow-through system. The short propagation lag (~1.8 months) and Granger causality across all 1–12 month lag windows are consistent with the response dynamics of river-connected shallow lakes globally (Barker et al., 2016; Huang et al., 2017; Li et al., 2024), and with the Zhou et al. (2024) synthesis characterising catchment buffering capacity as a primary filter governing meteorological-to-hydrological drought signal transfer.

### 4.4. Land cover divergence as the mechanism behind comparable non-climatic trends

Despite exhibiting broadly similar directional land-cover trajectories, cropland expansion and forest decline in both catchments, differing principally in magnitude, the two lakes show statistically indistinguishable rates of non-climatic hydrological deterioration: Theil-Sen residual slopes of −0.00646 SLLI month$^{-1}$ [95% CI: −0.00741 to −0.00564] at İznik and −0.00717 month$^{-1}$ [95% CI: −0.00777 to −0.00650] at Uluabat (Mann-Kendall $p < 0.0001$ for both). This convergence of absolute impact magnitude from mechanistically distinct anthropogenic pressures, principally irrigation-driven abstraction at İznik and direct river abstraction at Uluabat, is a novel finding of considerable management significance.

At Lake İznik, GLC_FCS30D reveals an expansion of cropland from 216.4 km² (15.5%) in 2000 to 245.1 km² (17.5%) in 2022 (+28.7 km², +13.3%), concurrent with a net decline in tree/forest cover from 616.6 km² (44.1%) to 579.7 km² (41.5%) (−36.9 km², −6.0%), representing the dominant land-cover transition in the catchment. Agricultural expansion elevates catchment-wide irrigation water demand, generating abstraction pressure on lake inflows independently of climatic forcing. Forest loss may further modulate

the runoff regime by reducing canopy interception and transpiration-driven subsurface recharge, though the net hydrological effect of forest cover change depends critically on site-specific soil and climate conditions, as emphasised by Shadmehri Toosi et al. (2025). The suppressor variable structure at İznik, the baseline SPEI-12/SLLI correlation rising from $r = 0.232$ to $r_{partial} = 0.289$ (95% CI: 0.195 to 0.379) after controlling for GLC_FCS30D-derived cropland area, indicates that agricultural expansion co-varies with the mechanisms suppressing lake inflow, creating a statistical confound that, when removed, reveals a modestly stronger underlying climate–lake coupling. Both correlations are statistically significant at $n = 384$, indicating partial rather than complete climate–lake decoupling.

At Lake Uluabat, cropland remained the dominant land-cover class and expanded only marginally from 472.4 km² (48.2%) to 480.3 km² (49.0%) (+7.9 km², +1.7%), while tree/forest cover declined modestly from 248.1 km² (25.3%) to 230.8 km² (23.5%). The minimal cropland trajectory renders agricultural expansion insufficient to account for the observed scale of non-climatic hydrological deterioration, and the dominant driver appears to be direct anthropogenic water abstraction from the Mustafakemalpaşa River, evidenced by four drought events (detailed in Table S11) occurring under neutral or positive concurrent SPEI-3 conditions. This pattern is consistent with Li et al. (2024) and Dai et al. (2025), who document LULC-mediated changes in drought propagation sensitivity and demonstrate that human water abstractions can generate hydrological drought independently of meteorological precursors.

The finding that cropland expansion and direct river abstraction produce comparable absolute rates of hydrological deterioration at adjacent lake systems underscores the point made by Luo et al. (2024) that the drought–LULC nexus is pathway-specific: identical outcomes may arise from entirely different process chains, requiring mechanistic rather than purely statistical attribution to guide adaptive management. Chen et al. (2025) extend this argument further, demonstrating that LULC change reshapes drought propagation in three dimensions, altering propagation angle and temporal structure alongside intensity, while precipitation and temperature primarily govern propagation distance, a finding structurally consistent with the basin-type-dependent propagation timescale contrasts documented between İznik and Uluabat in the present study.

### 4.5. Methodological contributions: GLEAM4, SNDWI validation, and PEI

This study makes three interconnected methodological contributions. First, the application of GLEAM4-derived PET in Mediterranean lake drought attribution resolves a long-standing bias problem in regional drought characterisation. GLEAM4's improved representation of interception loss for tall and short vegetation, atmospheric water demand via the Penman equation, and plant access to groundwater (Miralles et al., 2025) is particularly consequential for the İznik catchment, where the interplay between a declining but still dominant tree/forest cover class (579.7 km², 41.5% in 2022) and expanding cropland constitutes an evolving mosaic of evapotranspiration regimes. Even under net forest decline, transpiration from the remaining forest cover remains the largest vegetative component of the catchment water balance, and GLEAM4's capacity to resolve soil moisture stress and groundwater access across vegetation types improves the reliability of ET attribution in a landscape undergoing simultaneous deforestation and agricultural intensification.

Future studies applying temperature-only PET (Thornthwaite or similar) in this region should treat their SPEI outputs, and any propagation analyses derived from them, with caution: the Thornthwaite equation systematically underestimates PET in semi-arid and transitional climates by failing to account for aerodynamic and radiative drivers of evaporative demand, diverging most substantially from Penman-

Monteith at event scale and shorter accumulation periods (Kumari et al., 2024; Lee et al., 2024), and this will attenuate the evaporative demand signal and may misidentify the dominant drought driver.

Second, the SNDWI cross-validation analysis establishes a morphotype-specific rule of applicability for optical-index-based lake drought monitoring: Pearson $r = 0.451$ ($p < 0.001$) and SNDWI leading SLLI by 3 months at İznik confirm that, in deep, optically simple lakes, NDWI-based indices provide reliable independent cross-validation of altimetric drought assessments (Mahmood et al., 2025). At Uluabat, the consistently negative lag-correlations across all 13 tested offsets (with the most significant value at 12 months, $r = -0.265$, $p = 4.4 \times 10^{-4}$) are not a null result but an inversion, indicative of systematic optical complexity from macrophyte dynamics, sediment resuspension, and floodplain-wetland interactions that decouple surface reflectance from volumetric storage. This finding has direct implications for remote sensing-based global lake drought monitoring programs (Cheng et al., 2025), which should stratify optical index performance by lake morphotype before using NDWI-family indices as drought validators.

Third, the Propagation Efficiency Index (PEI), operationalized here as the fraction of antecedent meteorological drought events that successfully propagate to hydrological drought within a 24-month forward window, provides a dimensionless, basin-size-independent, and timescale-independent metric for cross-system comparison. Cross-correlation and run-theory frameworks have shown that propagation characteristics are shaped by catchment storage, LULC, and human regulation (Ikingura & Staniszewski, 2026; Li et al., 2024), but event-based efficiency fractions comparable to PEI remain uncommonly reported, limiting cross-system benchmarking. At Uluabat, PEI = 30.8% [95% CI: 15.4–48.7%]; at İznik, the four-event sample precludes reliable PEI computation by this method, itself a manifestation of İznik's extreme event scarcity under its current low-propagation-efficiency regime. The wide bootstrap confidence interval at Uluabat underscores the event-level uncertainty inherent in propagation fraction estimation from records of this length, and future work extending the record or pooling comparable lake systems could narrow this interval substantially.

### 4.6. Limitations and inferential boundaries

Several limitations bound the inferential scope of this study. First, the İznik SLLI exhibits non-stationarity (ADF $p = 0.061$, KPSS $p < 0.01$), technically violating the assumptions of Pearson cross-correlation significance testing and OLS regression. The Granger causality results at lag 12 months, confirmed by moving-block bootstrap with a 27-month block length ($p_{boot} = 0.031$ for SPEI-12), partially mitigate this concern by employing a resampling procedure that respects the series' serial dependence structure; nonetheless, all İznik propagation inferences must be regarded as directional and subject to confirmation from longer records or alternative estimation approaches designed for non-stationary time series. Second, the attribution OLS model for İznik ($R^2 = 0.306$; Durbin-Watson = 0.247) is affected by severe positive residual autocorrelation that invalidates conventional standard errors; HAC-corrected (Newey-West) inference is required before individual predictor t-statistics, including the nominally significant SPEI-24 coefficient ($\beta = +1.171$, $t = 6.47$), can be interpreted with confidence. Third, the climate-only attribution model for Uluabat explains only 12.2% of SLLI variance, with the unattributed 87.8% likely dominated by abstraction from the Mustafakemalpaşa River and intra-class management intensity changes, including irrigation scheduling and crop rotation, not captured by the GLC_FCS30D 30 m annual classification, which additionally may misclassify irrigated cropland transitions given the spectral similarity of irrigated and rainfed surfaces in optical imagery. Finally, the propagation analysis is conditioned on a common observational period (January 1993–December 2024) in which the pre-gauge altimetric record (1993–

1999 for İznik; 1993–2003 for Uluabat) relies on bias-corrected satellite altimetry with source weights estimated over the overlap period. While the leave-one-out stability analysis confirms SLLI robustness ($r = 0.998$ for both lakes), altimetric biases in the pre-gauge period cannot be fully excluded and may affect the characterisation of early drought events.

### 4.7. Regional implications and framework transferability

The broader implications of this study span both regional water resources management and global methodological applicability. Within the Marmara region, the attribution results define divergent management priorities at the two lakes. At Lake İznik, which serves as a drinking water reserve, the continued expansion of agricultural land, up 13.3% between 2000 and 2022, will progressively increase irrigation abstraction demand on catchment inflows independently of any precipitation trajectory. Concurrently, the ongoing net decline in tree/forest cover may alter runoff generation and subsurface recharge in ways that compound inflow suppression, though the direction of this effect depends on site-specific hydrological conditions. Long-term supply projections that rely solely on climate scenarios without accounting for these land-cover-driven abstraction and runoff changes will systematically overestimate available water.

At Lake Uluabat, the Ramsar-designated wetland whose level dynamics are closely coupled to irrigation abstraction from the Mustafakemalpaşa River, management of agricultural water demand is the primary lever for maintaining baseline hydrological conditions, particularly given that rising evaporative demand will progressively amplify the moisture deficit signal that drives agricultural abstraction. The absence of a significant precipitation trend at either lake means that observed and projected hydrological deterioration at both sites is, and will likely remain, primarily a function of increasing PET and human water use, not of precipitation change, a conclusion consistent with the regional drought intensification analysis of Kenawy et al. (2026) for the broader Middle East and North Africa. Methodologically, the all-satellite framework (CHIRPS v3, GLEAM4, HydroWeb/Sentinel-3, GLC_FCS30D) requires no in-situ discharge records, making it directly applicable to comparable lake pairs in Central Asia (endorheic basins), the East African Rift, and the Tibetan Plateau, where attribution challenges of equivalent complexity exist alongside sparse ground-based monitoring infrastructure. The dual-lake natural experiment design, in particular, offers an underexploited methodological opportunity in the limnological literature: when two geographically proximate lakes under equivalent atmospheric forcing diverge in their drought trajectories, the divergence provides a tractable basis for isolating basin-specific and land-cover-specific contributions without requiring counterfactual model simulations (Engman et al., 2025). Extending this framework to lake triads or clusters with systematic morphological gradients could further constrain the sensitivity of propagation efficiency to individual basin attributes.

## 5. Conclusions

This study set out to explain why two lakes separated by approximately 50 km, sharing an essentially identical precipitation climatology and the same regional evaporative demand, have followed markedly different hydrological drought trajectories over the past three decades. The natural experiment design, exploiting Lakes İznik and Uluabat as hydraulically independent, climatologically equivalent systems with divergent land cover histories, has produced a coherent and internally consistent attribution.

The first and most consequential finding concerns the climatic driver of drought intensification. Over 1981–2024, annual precipitation exhibited no statistically significant trend at either lake, while GLEAM4-

derived PET increased at rates of +2.90 mm $yr^{-1}$ at İznik and +3.35 mm $yr^{-1}$ at Uluabat, equivalent to cumulative increases of approximately 125 and 145 mm above baseline values. The practical consequence is stark: SPEI-12 drought frequency more than doubled at both sites between the 1981–2000 and 2001–2024 sub-periods, while SPI-12 frequency remained statistically unchanged. Rising evaporative demand, not declining precipitation, is therefore the primary mechanism behind observed drought intensification in these basins, and this conclusion would be invisible to any analysis relying on temperature-only Thornthwaite PET formulations. The first-ever application of GLEAM4 in this context confirms the necessity of physically consistent, radiation- and vapour-pressure-based PET estimates for attributing Mediterranean drought trends correctly.

The second major finding concerns the structural controls on drought propagation. Despite experiencing the same climatic forcing, the two lakes exhibit propagation characteristics that differ by nearly an order of magnitude in characteristic timescale. Lake Uluabat, an extremely shallow flow-through system with a large catchment-to-lake area ratio of ~40 and strong hydrological connectivity to the Mustafakemalpaşa River, responds to seasonal moisture deficits within approximately 1–2 months. Statistically significant cross-correlations with SPEI-3 and SPEI-6 ($r = 0.326$ and 0.315, respectively), Granger causality confirmed across all 1–12 month lag windows, and a bootstrap-estimated Propagation Efficiency Index of 30.8% collectively characterise Uluabat as a responsive, seasonally sensitive system. Lake İznik, by contrast, is a deep tectonic lake (~80 m maximum depth, catchment:lake area ratio ~5.7) whose SLLI exhibits a lag-1 autocorrelation of 0.927. Its level integrates atmospheric forcing over multi-year timescales; the dominant hydrological drought event (October 2020 – October 2023) required sustained concurrent deficits in both SPEI-12 and ultimately SPEI-24 before a persistent lake-level response emerged, with a propagation lag of approximately 9–10 months from the onset of the antecedent 12-month drought signal. The absence of statistically significant cross-correlations at İznik reflects a structural inferential constraint, severe effective sample size reduction imposed by the SLLI's persistence, rather than the absence of physical coupling, as the Granger causality result at lag 12 (bootstrap-confirmed $p_{boot} = 0.031$) demonstrates. Together, these results confirm that basin morphology and hydrological connectivity are primary determinants of propagation regime, capable of producing near-order-of-magnitude differences in drought transmission timescale between geographically proximate systems under equivalent atmospheric forcing.

The third finding resolves the anthropogenic contribution. GLC_FCS30D-derived land-cover analysis over 2000–2022 reveals that both basins underwent cropland expansion and forest decline, but at contrasting magnitudes and with distinct operative mechanisms: at İznik, agricultural area expanded by 13.3% (+28.7 $km^2$) while tree/forest cover declined by 36.9 $km^2$ (−6.0%), with irrigation abstraction constituting the primary inflow-suppression mechanism; at Uluabat, cropland expanded only marginally (+1.7%, +7.9 $km^2$) and direct abstraction from the Mustafakemalpaşa River constitutes the dominant non-climatic stressor. Despite these mechanistically distinct pathways, Mann-Kendall analysis of SPEI-12 residual SLLI trends yields statistically indistinguishable rates of non-climatic hydrological deterioration at the two lakes (Theil-Sen slopes: −0.0065 SLLI $month^{-1}$ at İznik and −0.0072 $month^{-1}$ at Uluabat; overlapping 95% confidence intervals). This convergence of outcome magnitude from distinct process chains is a novel and practically important finding: it underscores that agricultural expansion with associated irrigation abstraction and direct river diversion can produce equivalent long-term pressure on lake water balances, and that inferring the operative mechanism from the rate of decline alone is not possible without process-based attribution.

Three methodological contributions follow from these findings. First, the Propagation Efficiency Index provides a dimensionless, basin-size-independent metric for cross-system comparison of meteorological-to-hydrological drought transmission that does not require discharge records. Second, the SNDWI cross-validation results establish a morphotype-specific applicability rule for optical index-based lake drought monitoring: NDWI-based indices perform well in deep, optically clear lakes (İznik: Pearson $r = 0.451$, $p < 0.001$) but are systematically unreliable in shallow, turbid, macrophyte-dominated systems (Uluabat: lag-correlations consistently negative across all 13 tested offsets), a finding with direct implications for global remote sensing-based lake drought monitoring programmes. Third, the dual-lake natural experiment design exploits a genuinely underused methodological opportunity: when two climatologically equivalent lakes diverge in their drought trajectories, the divergence itself functions as a controlled attribution signal without requiring counterfactual model simulations.

From a management perspective, the results define divergent priorities at the two sites. At Lake İznik, a drinking water reserve, the ongoing trajectory of agricultural expansion and associated irrigation abstraction will continue to suppress catchment inflows independently of any future precipitation trajectory, and long-term supply projections that rely solely on climate scenarios without accounting for land-cover-driven abstraction changes will systematically overestimate available water. At Lake Uluabat, a Ramsar-designated wetland, agricultural water demand management is the primary intervention lever for maintaining baseline hydrological conditions, given that rising evaporative demand will progressively amplify the moisture deficit signal that drives irrigation abstraction. Crucially, at neither lake does the observed or projected hydrological deterioration appear to be primarily driven by precipitation change: it is the combination of steadily rising evaporative demand and structural anthropogenic pressures, irrigation abstraction at İznik and direct river diversion at Uluabat, that defines the trajectory at both sites.

Finally, the all-satellite framework demonstrated here, drawing on CHIRPS v3, GLEAM4, satellite altimetry, and GLC_FCS30D, with no dependence on in-situ discharge records, is directly applicable to lake systems in data-sparse regions including endorheic basins in Central Asia, the East African Rift Valley, and the Tibetan Plateau, where attribution challenges of comparable complexity are presently unresolvable by conventional monitoring-dependent methods. Extending the dual-lake or multi-lake natural experiment design to systems with more systematic morphological gradients offers a particularly promising avenue for further constraining the sensitivity of propagation efficiency to individual basin attributes across climate zones.

## Author contributions

A.M.A. conceived the study and developed the methodology, performed the software implementation, formal analysis, data curation, and validation, and prepared the visualizations. A.M.A. wrote the original draft of the manuscript. F.Ö. supervised the research, acquired funding, provided resources, and administered the project. F.Ö. reviewed and edited the manuscript. All authors read and approved the final manuscript.


## Acknowledgements

The authors gratefully acknowledge the Turkish Directorate General of State Hydraulic Works (DSİ) for providing the hydrological data used in this study. The authors also express their sincere gratitude to

Professor Hasan ÖZDEMİR for his valuable guidance, insightful discussions, and constructive comments throughout this research, which significantly improved the quality of the study.

## Data Availability Statement

GLC_FCS30D global land cover data are freely available from the Aerospace Information Research Institute, Chinese Academy of Sciences (AIR-CAS). CHIRPS v3 precipitation data are freely available at https://chc.ucsb.edu/data/chirps. GLEAM v4 evapotranspiration data are available at https://www.gleam.eu. Satellite altimetry data are available from HydroWeb (https://hydroweb.next.theia-land.fr/). Landsat imagery is available through Google Earth Engine. Processed index time series, analysis code, and other derived datasets generated during this study will be made available by the corresponding author upon reasonable request.

## Funding

This study was supported by Bursa Uludağ University Scientific Research Projects Coordination Unit under the General Research Project scheme (Project No. FGA-2025-2484).

## Clinical trial number

Not applicable.

## References

Abu Arra, A., & Şişman, E. (2024). A comprehensive analysis and comparison of SPI and SPEI for spatiotemporal drought evaluation. *Environmental Monitoring and Assessment*, *196*(10), 980. https://doi.org/10.1007/s10661-024-13127-7

Amiri, A. M., & Örüç, F. (2026). Basin runoff calibration using gradient boosting decision trees: Impact of dual gridded potential evapotranspiration sources on model performance in Iznik Lake Basin, Türkiye. *Journal of Hydrology: Regional Studies*, *66*, 103574. https://doi.org/10.1016/j.ejrh.2026.103574

Baigaliyeva, M., Mount, N., Gosling, S. N., & McGowan, S. (2024). Unravelling long-term impact of water abstraction and climate change on endorheic lakes: A case study of Shortandy Lake in Central Asia. *PLOS ONE*, *19*(7), e0305721. https://doi.org/10.1371/journal.pone.0305721

Barker, L. J., Hannaford, J., Chiverton, A., & Svensson, C. (2016). From meteorological to hydrological drought \hack\newline using standardised indicators. *Hydrology and Earth System Sciences*, *20*(6), 2483–2505. https://doi.org/10.5194/hess-20-2483-2016

Benjamini, Y., & Hochberg, Y. (1995). Controlling the False Discovery Rate: A Practical and Powerful Approach to Multiple Testing. *Journal of the Royal Statistical Society. Series B (Methodological)*, *57*(1), 289–300. JSTOR.

Bevacqua, E., Rakovec, O., Schumacher, D. L., Kumar, R., Thober, S., Samaniego, L., Seneviratne, S. I., & Zscheischler, J. (2024). Direct and lagged climate change effects intensified the 2022 European drought. *Nature Geoscience*, *17*(11), 1100–1107. https://doi.org/10.1038/s41561-024-01559-2

Bouabdelli, S., Massari, C., Morlot, M., Castelli, M., & Formetta, G. (2025, March 15). *High-Resolution (1km Daily) Potential Evapotranspiration Dataset Over Europe and the Mediterranean Region*. https://doi.org/10.5194/egusphere-egu25-18052

Brands, S., Iturbide, M., Díez González-Pardo, J., Herrera, S., Bedia, J., Manzanas, R., Rodríguez-Guisado, E., Beguería, S., Vicente-Serrano, S. M., & Gutiérrez, J. M. (2025). Seasonal drought predictions in the Mediterranean using the SPEI index: Paving the way for their operational applicability in climate services. *Climate Services*, *38*, 100555. https://doi.org/10.1016/j.cliser.2025.100555

Bretherton, C. S., Widmann, M., Dymnikov, V. P., Wallace, J. M., & Bladé, I. (1999). The Effective Number of Spatial Degrees of Freedom of a Time-Varying Field. *Journal of Climate*, *12*(7), 1990–2009. https://doi.org/10.1175/1520-0442(1999)012%3C1990:TENOSD%3E2.0.CO;2

Chandy, M., Schifano, E. D., Yan, J., & Zhang, X. (2026). Nonparametric Block Bootstrap Kolmogorov-Smirnov Goodness-of-Fit Test. *The American Statistician*, *80*(2), 241–248. https://doi.org/10.1080/00031305.2025.2588131

Chelton, D. B. (1983). Effects of sampling errors in statistical estimation. *Deep Sea Research Part A. Oceanographic Research Papers*, *30*(10), 1083–1103.

Chen, H., Meng, F., Sa, C., Luo, M., Bao, Y., & Liu, T. (2025). A three-dimensional perspective on how land use/cover change reshapes drought propagation under climate change? *Journal of Hydrology: Regional Studies*, *60*, 102478. https://doi.org/10.1016/j.ejrh.2025.102478

Cheng, X., Wang, S., Chen, J., & AghaKouchak, A. (2025). Global assessment and hotspots of lake drought. *Communications Earth & Environment*, *6*(1), 308. https://doi.org/10.1038/s43247-025-02285-2

Climate Hazards Center. (2025). *Infrared Precipitation with Stations version 3 (CHIRPS3) Data Repository* [Dataset]. https://doi.org/https://doi.org/10.15780/G2JQ0P

Dai, M., Feng, P., Li, J., Shi, X., & Wang, H. (2025). Effects of land use/cover change on propagation dynamics from meteorological to soil moisture drought considering nonstationarity. *Agricultural Water Management*, *312*, 109452. https://doi.org/10.1016/j.agwat.2025.109452

Eekhout, J. P. C., Nunes, J. P., Tramblay, Y., & de Vente, J. (2025). Severe Impacts on Water Resources Projected for the Mediterranean Basin. *WIREs Water*, *12*(2), e70012. https://doi.org/10.1002/wat2.70012

Elmaci, A., Topaç, F. O., Ozengin, N., Teksoy, A., Kurtoglu, S., & Başkaya, H. S. (2008). Evaluation of physical, chemical and microbiological properties of lake Uluabat, Turkey. *Journal of Environmental Biology*, *29 2*, 205–210.

Engman, F., Kortekaas, E., Brandimarte, L., & Mazzoleni, M. (2025). Exploring land cover change after prolonged droughts at the global level. *Scientific Reports*, *15*(1), 28520. https://doi.org/10.1038/s41598-025-14713-6

Erkoç, M. H., Dogan, U., Keser, B., & Bayram, B. (2024). Temporal Hydrological Drought Analysis in Lake Iznik Using In-Situ Measurements and Space-Based Data. *Acta Geodynamica et Geomaterialia*, *22*, 1–15. https://doi.org/10.13168/AGG.2025.0001

Funk, C., Peterson, P., Harrison, L., Saldivar, R., Landsfeld, M., Pedreros, D., Shukla, S., Fink, A. H., Davenport, F., Peterson, S., Turner, W., Sonnier, A., Budde, M., Tabor, K., Verdin, J., Hauzaree, D., Naim, M., Alaso, D., & Husak, G. (2026). The Climate Hazards Center Infrared Precipitation with Stations, Version 3. *Scientific Data*, *13*(1), 718. https://doi.org/10.1038/s41597-026-07096-4

Gastineau, R., Anselmetti, F. S., Fabbri, S. C., Sabatier, P., Roeser, P., Gündüz, S., Şahin, M., Duarte, E., Rapuc, W., Gebhardt, A. C., Franz, S. O., Niessen, F., & de Sigoyer, J. (2024). Seismic stratigraphy and sediment cores reveal lake-level fluctuations in Lake Iznik (NW Turkey) over the past ~70 ka. *Sedimentary Geology*, *464*, 106620. https://doi.org/10.1016/j.sedgeo.2024.106620

Gebrechorkos, S. H., Sheffield, J., Vicente-Serrano, S. M., Funk, C., Miralles, D. G., Peng, J., Dyer, E., Talib, J., Beck, H. E., Singer, M. B., & Dadson, S. J. (2025). Warming accelerates global drought severity. *Nature*, *642*(8068), 628–635. https://doi.org/10.1038/s41586-025-09047-2

Gumus, V., & Seker, M. (2024). Projection of meteorological drought in Türkiye's Mediterranean region based on multi-model ensemble from CMIP6. *Hydrological Sciences Journal*, *69*(9), 1228–1243. https://doi.org/10.1080/02626667.2024.2364712

Huang, S., Li, P., Huang, Q., Leng, G., Hou, B., & Ma, L. (2017). The propagation from meteorological to hydrological drought and its potential influence factors. *Journal of Hydrology*, *547*, 184–195. https://doi.org/10.1016/j.jhydrol.2017.01.041

Ikingura, A., & Staniszewski, R. (2026). Spatio-Environmental Drivers of Water Scarcity in Semi-Arid Catchments: Insights from NDWI and LULC. *Water*, *18*(7), 855. https://doi.org/10.3390/w18070855

IPCC. (2021). Climate Change 2021: The Physical Science Basis. *Contribution*.

Kenawy, A. E., Al-Awadhi, T., Abdullah, M., Ostermann, F. O., & Abulibdeh, A. (2026). A Multidecadal Assessment of Drought Intensification in the Middle East and North Africa: The Role of Global

Warming and Rainfall Deficit. *Earth Systems and Environment*, *10*(1), 343–362. https://doi.org/10.1007/s41748-025-00576-4

Kumari, P., Shaik, R., Vannam, S. C., & Singh, S. K. (2024). Drought evaluation using various evapotranspiration models over semi-arid river basins. *Journal of Water and Climate Change*, *15*(8), 3582–3601. https://doi.org/10.2166/wcc.2024.699

Leader, S., Kettridge, N., Hannah, D. M., Mendoza, C., & Devito, K. J. (2024). Multi-year climate memory in shallow lake water levels. *Journal of Hydrology*, *642*, 131764. https://doi.org/10.1016/j.jhydrol.2024.131764

Lee, S., Moriasi, D. N., Danandeh Mehr, A., & Mirchi, A. (2024). Sensitivity of Standardized Precipitation and Evapotranspiration Index (SPEI) to the choice of SPEI probability distribution and evapotranspiration method. *Journal of Hydrology: Regional Studies*, *53*, 101761. https://doi.org/10.1016/j.ejrh.2024.101761

Li, Y., Huang, Y., Li, Y., Zhang, H., Fan, J., Deng, Q., & Wang, X. (2024). Spatiotemporal heterogeneity in meteorological and hydrological drought patterns and propagations influenced by climatic variability, LULC change, and human regulations. *Scientific Reports*, *14*(1), 5965. https://doi.org/10.1038/s41598-024-56526-z

Luo, Y., Chen, R., Yang, K., Zhou, X., Jia, T., Shang, C., Pei, X., Wang, Q., Li, D., Peng, C., & Guo, H. (2024). Response of changes in lake area to drought and land use change. *Science of The Total Environment*, *947*, 174638. https://doi.org/10.1016/j.scitotenv.2024.174638

Mahmood, M. R., Abrahem, B. I., Jumaah, H. J., Alalwan, H. A., & Mohammed, M. M. (2025). Drought monitoring of large lakes in Iraq using remote sensing images and normalized difference water index (NDWI). *Results in Engineering*, *25*, 103854. https://doi.org/10.1016/j.rineng.2024.103854

Massey, F. J. (1951). The Kolmogorov-Smirnov Test for Goodness of Fit. *Journal of the American Statistical Association*, *46*(253), 68–78. JSTOR. https://doi.org/10.2307/2280095

Mckee, T. B., Doesken, N. J., & Kleist, J. R. (1993). *THE RELATIONSHIP OF DROUGHT FREQUENCY AND DURATION TO TIME SCALES*. 179–184. https://api.semanticscholar.org/CorpusID:129950974

Miao, C., Zhang, Q., Li, X., Hu, J., Sadegh, M., & AghaKouchak, A. (2026). Global drought extremes in 2025. *Nature Reviews Earth & Environment*. https://doi.org/10.1038/s43017-026-00785-z

Miralles, D. G., Bonte, O., Koppa, A., Baez-Villanueva, O. M., Tronquo, E., Zhong, F., Beck, H. E., Hulsman, P., Dorigo, W., Verhoest, N. E. C., & Haghdoost, S. (2025). GLEAM4: Global land evaporation and soil moisture dataset at 0.1° resolution from 1980 to near present. *Scientific Data*, *12*(1), 416. https://doi.org/10.1038/s41597-025-04610-y

Mwinjuma, M., Wang, R., Mtupili, M., & Twaha, M. (2026). Comparisons of SPI and SPEI in capturing drought dynamics: A Global assessment across arid and humid regions. *Atmospheric Research*, *329*, 108475. https://doi.org/10.1016/j.atmosres.2025.108475

Nwayor, I. J., & Robeson, S. M. (2024). Exploring the relationship between SPI and SPEI in a warming world. *Theoretical and Applied Climatology*, *155*(4), 2559–2569. https://doi.org/10.1007/s00704-023-04764-y

Quenouille, M. H. (1952). *Associated measurements.*

Ramachandran, J., Rashwin, A. A., Arunadevi, K., Lalitha, R., Kannan, S. V., Sivasubramanian, K., & Kannan, B. (2026). Investigation of 50 temperature-based models for estimating potential evapotranspiration (PET) in a semi-arid region. *Scientific Reports*, *16*(1), 7879. https://doi.org/10.1038/s41598-026-35472-y

Rezaei, A., Karami, K., Tilmes, S., & Moore, J. C. (2024). Future water storage changes over the Mediterranean, Middle East, and North Africa in response to global warming and stratospheric aerosol intervention. *Earth System Dynamics*, *15*(1), 91–108. https://doi.org/10.5194/esd-15-91-2024

Seager, R., Wu, Y., Cherchi, A., Simpson, I. R., Osborn, T. J., Kushnir, Y., Lukovic, J., Liu, H., & Nakamura, J. (2024). Recent and near-term future changes in impacts-relevant seasonal hydroclimate in the world's Mediterranean climate regions. *International Journal of Climatology*, *44*(11), 3792–3820. https://doi.org/10.1002/joc.8551

Shadmehri Toosi, A., Batelaan, O., Shanafield, M., & Guan, H. (2025). Land Use-Land Cover and Hydrological Modeling: A Review. *WIREs Water*, *12*(2), e70013. https://doi.org/10.1002/wat2.70013

Sheffield, J., Wood, E. F., & Roderick, M. L. (2012). Little change in global drought over the past 60 years. *Nature*, *491*(7424), 435–438. https://doi.org/10.1038/nature11575

Soydan, O. (2026). Climate-Induced Evaporation and Salinity Dynamics in Southwestern Türkiye's Endorheic Lakes: A Multi-Year Remote Sensing and Hydrostatistical Analysis. *Rocznik Ochrona Środowiska*, *28*, 139–152. https://doi.org/10.54740/ros.2026.011

Stagge, J. H., Tallaksen, L. M., Gudmundsson, L., Van Loon, A. F., & Stahl, K. (2015). Candidate Distributions for Climatological Drought Indices (SPI and SPEI). *International Journal of Climatology*, *35*(13), 4027–4040. https://doi.org/10.1002/joc.4267

Tagil, S. (2007). Quantifying the Change Detection of the Uluabat Wetland, Turkey, by Use of Landsat Images. *Ekoloji*, *16*, 9–20.

Van Loon, A. F., Kchouk, S., Matanó, A., Tootoonchi, F., Alvarez-Garreton, C., Hassaballah, K. E. A., Wu, M., Wens, M. L. K., Shyrokaya, A., Ridolfi, E., Biella, R., Nagavciuc, V., Barendrecht, M.

H., Bastos, A., Cavalcante, L., de Vries, F. T., Garcia, M., Mård, J., Streefkerk, I. N., … Werner, M. (2024). Review article: Drought as a continuum: Memory effects in interlinked hydrological, ecological, and social systems. *EGUsphere*, *2024*, 1–78. https://doi.org/10.5194/egusphere-2024-421

Vicente-Serrano, S. M., Beguería, S., & López-Moreno, J. I. (2010). A Multiscalar Drought Index Sensitive to Global Warming: The Standardized Precipitation Evapotranspiration Index. *Journal of Climate*, *23*(7), 1696–1718. https://doi.org/10.1175/2009JCLI2909.1

Vicente-Serrano, S. M., Peña-Angulo, D., Beguería, S., Domínguez-Castro, F., Tomás-Burguera, M., Noguera, I., Gimeno-Sotelo, L., & El Kenawy, A. (2022). Global drought trends and future projections. *Philosophical Transactions of the Royal Society A: Mathematical, Physical and Engineering Sciences*, *380*(2238), 20210285. https://doi.org/10.1098/rsta.2021.0285

WMO. (2012). *Standardized Precipitation Index User Guide*. World Meteorological Organization.

Xiong, H., Han, J., & Yang, Y. (2025). Propagation From Meteorological to Hydrological Drought: Characteristics and Influencing Factors. *Water Resources Research*, *61*(4), e2024WR037765. https://doi.org/10.1029/2024WR037765

Yao, F., Livneh, B., Rajagopalan, B., Wang, J., Crétaux, J.-F., Wada, Y., & Berge-Nguyen, M. (2023). Satellites reveal widespread decline in global lake water storage. *Science*, *380*(6646), 743–749. https://doi.org/10.1126/science.abo2812

Zhang, X., Zhao, T., Xu, H., Liu, W., Wang, J., Chen, X., & Liu, L. (2024). GLC_FCS30D: the first global 30\,m land-cover dynamics monitoring product with a fine classification system for the period from 1985 to 2022 generated using dense-time-series Landsat imagery and the continuous change-detection method. *Earth System Science Data*, *16*(3), 1353–1381. https://doi.org/10.5194/essd-16-1353-2024

Zhao, G., Gao, H., Li, Y., Tang, Q., Woolway, R. I., Merder, J., Rosa, L., & Michalak, A. M. (2025). Decoupling of surface water storage from precipitation in global drylands due to anthropogenic activity. *Nature Water*, *3*(1), 80–88. https://doi.org/10.1038/s44221-024-00367-7

Zhou, Z., Wang, P., Li, L., Fu, Q., Ding, Y., Chen, P., Xue, P., Wang, T., & Shi, H. (2024). Recent development on drought propagation: A comprehensive review. *Journal of Hydrology*, *645*, 132196. https://doi.org/10.1016/j.jhydrol.2024.132196

1136

## Supplementary Files

This is a list of supplementary files associated with this preprint. Click to download.

- AmiriOrucSupplementary.docx